FEMORAL HEAD SECONDARY CENTER OF OSSIFICATION DEVELOPMENT IN A CANINE MODEL OF HIP DYSPLASIA: ONSET, MINERAL DENSITY, AND SHAPE

A Dissertation

Presented to the Faculty of the Graduate School

of Cornell University

In Partial Fulfillment of the Requirements for the Degree of

Doctor of Philosophy

by

Wendy S. Vanden Berg-Foels

August 2007

FEMORAL HEAD SECONDARY CENTER OF OSSIFICATION DEVELOPMENT IN A CANINE MODEL OF HIP DYSPLASIA: ONSET, MINERAL DENSITY, AND SHAPE

Wendy S. Vanden Berg-Foels, Ph.D.

Cornell University 2007

Developmental dysplasia of the hip (DDH) is characterized by joint subluxation, malformation, and early onset osteoarthritis. Little is known about how increased body weight and chronic subluxation affect the course of early postnatal hip development. The objective of this research was to test the association of body weight and subluxation with femoral head mineral density and shape development, and with joint degeneration at early adulthood.

A longitudinal study was conducted using a canine model of DDH. Serial body weight, age at femoral head ossification onset, and femoral head coverage at 16 and 32 weeks were measured. Bone mineral density and secondary center of ossification (SCO) shape were evaluated noninvasively using serial quantitative computed tomography at 7 ages between 4 to 32 weeks. Weight and shape analyses were conducted with 34 hips; mineral density analysis was conducted with 28 hips. Degeneration at 32 weeks was assessed using necropsy and cartilage biochemistry.

There was a negative association between birth weight and age at femoral head ossification onset; however, the association was likely due to skeletal maturity level rather than body weight *per se*. Lower birth weight subjects had greater femoral head

coverage at 16 weeks. Greater birth weight was associated with greater probability of degenerative changes at 32 weeks. During growth acceleration, greater subluxation was associated with a lower mean SCO density, and, at 32 weeks, with a greater peak density and a greater area of high density subchondral bone in a more lateral location. Subluxation was also associated with a greater probability of degenerative changes at 32 weeks. At 14 and 32 weeks, greater subluxation was associated with a thinner SCO in the perifoveal region, the characteristic site of lesion formation. Increased thinness was associated with a greater probability of degenerative changes. At 32 weeks, greater subluxation was also associated with a greater bend in the SCO lateral to the perifoveal region.

These results support the hypothesis that increased birth weight and chronic subluxation during the critical early postnatal growth period are sufficient to alter SCO density distribution and shape during development and result in measurable degenerative changes at adulthood.

BIOGRAPHICAL SKETCH

Wendy was born in the small town of Canton, South Dakota, and grew up on a farm across the border in Northwest Iowa. Farm life introduced her to hard work at a very early age, and, in addition to no television, provided endless opportunity for expression of initiative and creativity. Wendy had to create her own fun. Even as a child, she was always curious about how things worked; she was constantly assembling or disassembling something.

Despite her abundant intellectual curiosity, Wendy may not have considered attending college had she not been nominated for the Talent Search Program sponsored by Central College. With their encouragement, she applied, and was admitted, to the University of Iowa. In 1994, she was awarded a Bachelor of Science degree in Mechanical Engineering, with honors and high distinction. In 1998, she was awarded a Master of Science degree in Mechanical Engineering from Cornell University.

Wendy's evolving interests in interdisciplinary research lead her to change her field from Mechanical to Biomedical Engineering for her Ph.D. research. During her Ph.D. candidacy, Wendy faced several personal challenges including the death of her grandparents and mother, greater family obligations as a result of her mother's death, and an extended illness. In what may be an example of Friedrich Nietzsche's assertion "Whatever does not kill me, makes me stronger", she dealt with the losses and responsibilities, regained her health, and returned to complete her Ph.D. research. At the beginning of this journey, Wendy did not know that an interdisciplinary approach to the research of skeletal development would be her passion; however, through the process of exploration and discovery, she is exactly where she should be.

In memory of my grandparents and mother,

Cornelius, Nellie, and Marlys Vanden Berg

ACKNOWLEDGMENTS

I accomplished my Ph.D. research with support and guidance from many sources. I was funded by a National Science Foundation Fellowship and an American Association of University Women Selected Professions Fellowship. Funding to carry out this research was provided by a New York State Advanced Technology Biotechnology Program grant and two grants from the Cornell University College of Veterinary Medicine Consolidated Research Grant Program. As a student, I could not be a principal investigator; however, Dr. Todhunter gave me the freedom to write and administer the grants. This experience will serve me well.

The research technicians I worked with passed on a wealth of practical knowledge. Barb Chapman, Liz Corey, and Mary Lou Norman, your help was appreciated. Margaret Vernier-Singer deserves a special thank you for supporting my research in so many ways.

Transitioning from Mechanical to Biomedical Engineering after my A-exam was not without difficulty. I owe a special debt of gratitude to Dr. Terry Plater, Associate Dean of Academic Affairs for the Graduate School, and to Dr. Mike Kelley, Associate Dean of Professional Development for the College of Engineering, for their support and guidance. I am most grateful to Dr. Michael Shuler, Director of the Biomedical Engineering Program, and Dr. William Olbricht, Director of Graduate Studies, for granting my petition to pursue a Ph.D. in Biomedical Engineering.

I have been fortunate to work and learn with so many dedicated and supportive students. There are simply too many to list here. Thank you, Andinet Enquobahari, for such great camaraderie.

My family and friends have also taken this journey with me. Thank you, Rob Foels, for being my best friend and partner in life. Ruth and Ken Kooima, you are one terrific aunt and uncle. Thank you to my little sister Amanda who now worries about me, and to my brother Shannon for sending all those jokes. The support and encouragement of my dear friend Meg Holloway has been a blessing. Thank you, Adriano Manocchia, for your support, both personal and technical.

Finally, I would like to thank my committee, Drs. Anthony P. Reeves, Rory J. Todhunter, and James T. Jenkins. I also want to extend a special thank you to Dr. Steven J. Schwager who has served essentially as a fourth committee member. This experience would not have been possible without your guidance and support.

TABLE OF CONTENTS

LIST OF FIGURES

LIST OF TABLES

LIST OF ABBREVIATIONS

BMD	bone mineral density
DDH	developmental dysplasia of the hip
EGR	exponential growth rate
GAG	glycosaminoglycan
HLM	hierarchical linear model
MLL	medial-lateral location
m-rep	medial representation
NR	normalized radius
NZH	normalized z-axis height
OA	osteoarthritis
PC/PCA	principal component/principal component analysis
QCT	quantitative computed tomography
SCO	secondary center of ossification

CHAPTER 1

EFFECT OF EARLY POSTNATAL BODY WEIGHT ON FEMORAL HEAD OSSIFICATION ONSET AND HIP OSTEOARTHRITIS IN A CANINE MODEL OF DEVELOPMENTAL DYSPLASIA OF THE HIP[1]

Abstract

Developmental dysplasia of the hip (DDH) is a well-known precipitator of hip osteoarthritis. An increase in body weight during the critical early postnatal growth period may alter joint contact, and thus alter hip development and influence joint health in adulthood. The objective of this study was to determine whether early postnatal body weight affected the course of hip development and the onset of osteoarthritis in a canine model of DDH. A longitudinal study, from birth to skeletal maturity, was conducted. Serial body weight, age at femoral head ossification onset, and femoral head coverage at 4 months were measured. Presence and severity of degeneration at 8 months were determined using necropsy and cartilage biochemistry. There was a negative association between birth weight and age at femoral head ossification onset; however, the association was likely due to skeletal maturity level rather than body weight *per se*. Lower birth weight subjects had greater femoral head coverage at 4 months. Greater birth weight was associated with greater probability of moderate degenerative changes or macroscopic lesions at 8 months. These results support the hypothesis that increased birth weight is sufficient to alter the course of hip development and result in measurable degenerative changes at adulthood.

[1] Vanden Berg-Foels WS, Todhunter RJ, Schwager SJ, Reeves AP 2006 Effect of early postnatal body weight on femoral head ossification onset and hip osteoarthritis in a canine model of developmental dysplasia of the hip. Pediatr Res 60:549-554

Introduction

Developmental dysplasia of the hip (DDH), characterized in the adult by a shallow acetabulum and a flattened femoral head, is a well-known precipitator of early onset hip osteoarthritis (OA) (1-3). In the human neonate (4) and juvenile dog (5), DDH ranges from joint instability to complete dislocation of the femoral head.

Incidence estimates for DDH in humans vary with examination technique, child age, and disease definition; the true incidence is unknown (1,4). Screening surveys suggest that as many as 1 in 100 newborns have evidence of hip instability (4). Twenty percent to 50% of idiopathic OA cases have been attributed to underlying subluxation or acetabular dysplasia (1). Risk of DDH is greater for first borns, breech position, female gender, left hips, an adverse intrauterine environment such as oligohydramnios, and infants swaddled in a leg-extended position (1,4). Greater risk of left hip DDH is likely a result of two thirds of vertex presentations being in the left occiput position (1,6). Abduction of the left hip is limited as the fetus is pressed against the mother's spine resulting in decreased coverage of the femoral head by the acetabulum (7). Risk is also greater for positive family history (affected parent 12%; affected parent and sibling 36%) (1).

Incidence estimates for DDH in dogs vary by breed, and are greater for larger breeds. Approximately 20% of Labrador retrievers, a large breed, are affected; incidence exceeds 50% for St. Bernards (8). Heritability estimates range from 0.25 to 0.40 (9).

The dog is an established, naturally occurring model for the study of early onset OA secondary to DDH and shares the characteristic morphological and biochemical features of DDH in humans (1,5,9). A gender difference in incidence has not been

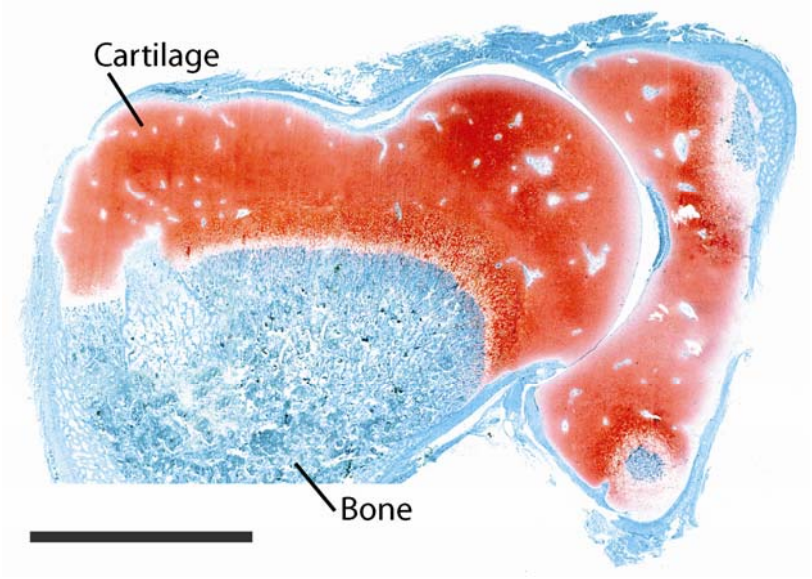

Figure 1.1 Hip at 1 day of age. Bar = 5 mm.

demonstrated in the dog model, and incidence is greater for larger breeds than for humans. Dogs are skeletally mature by 8 months, enabling longitudinal observation of DDH from incipience to degeneration.

A critical stage in hip development occurs during the early postnatal period. In humans, the depth of the acetabulum relative to its diameter is a minimum at birth, requiring that the joint capsule and ligament of the femoral head play a greater role in maintaining stability and congruent articulation (7). Although no comparable study exists for dogs, the capsule and ligament of the femoral head are largely responsible for maintaining congruent articulation for the first month after birth (5). Experimental animal models have demonstrated that fully congruent contact between the cartilaginous femoral head and acetabulum (Figure 1.1 morphology) is necessary for development of normal joint morphology (10,11) and that the neonatal joint has a remarkable capacity to respond to the local mechanical environment (12). In a rat model with a unilateral amputation below the femoral neck, presence of the femoral

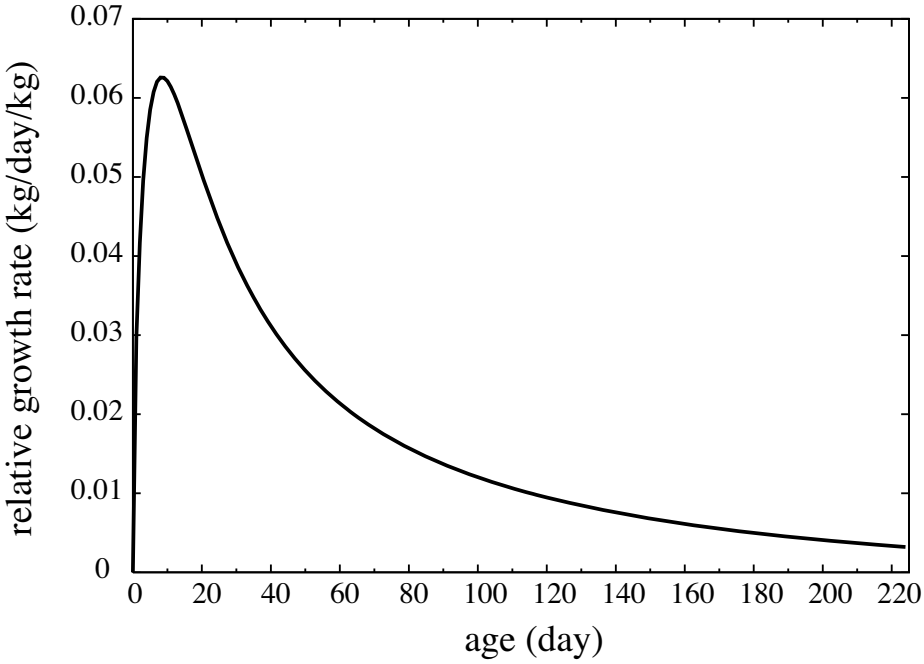

Figure 1.2 Rate of growth for body weight normalized by concurrent weight (study example).

head within the acetabulum was sufficient to retain congruent articulating surfaces (11). The rate of growth *relative to size* is at a maximum during the early postnatal period (Figure 1.2). Small perturbations in joint contact during the critical early postnatal growth period may alter the course of hip development and may influence joint health in adulthood.

Increased body weight during later development and early adulthood has been associated with a greater risk of hip OA. Increased body weight after 2 months of age in dogs has been associated with a more severe expression of DDH (13) and a greater prevalence of subsequent hip OA (14). A modest increase in body mass index at 18 years in humans was associated with an increased risk of hip OA leading to joint replacement (15). However, the effect of increased body weight during early postnatal

development, when congruent articulation is largely maintained by connective tissues, has not been investigated.

The objective of this study was to determine whether early postnatal body weight affected the course of hip development and the onset of OA in a canine model of DDH. We hypothesized that greater body weight during the first 3 weeks after birth would result in an earlier age at ossification onset, reduced femoral head coverage at 4 months, and greater probability of degenerative changes at 8 months.

Methods

Animals

Labrador retrievers were obtained from a colony maintained by the Baker Institute for Animal Health, Cornell University. Dogs were randomly selected from first available litters (phenotype of both sire and dam was either dysplastic or normal). The pattern of inheritance for hip morphology is complex. Dysplastic offspring from phenotypically normal parents, and *vice versa*, are common. Between 2 and 4 dogs were selected from 5 litters, resulting in a total of 17 subjects (Table 1.1).

Pups were introduced to solid food at 4 weeks and were weaned at 6 weeks; feeding was *ad libitum* thereafter. Body weight was recorded daily for the first three weeks. Enclosures provided area for exercise. The Cornell University Institutional Animal Care and Use Committee approved all aspects of this study.

Table 1.1 Sample Summary

Parental Phenotype	Litter	Gender	Litter Size
Dysplastic	1	2 female	8
	2	1 female, 2 male	8
	3	2 female, 2 male	9
Normal	4	2 female, 2 male	12
	5	2 female, 2 male	7

Radiography for Onset of Ossification

The pelvis was radiographed in a ventro-dorsal, hip-extended position (16). Radiographs were obtained every second day beginning at day 6 until ossification was observed in both femoral capital epiphyses. The age at which ossification was first observed for each femoral capital epiphysis was recorded as the age at ossification onset.

Radiography for Femoral Head Coverage

The dorso-lateral subluxation procedure (17) was used to measure femoral head coverage at 4 months. Dogs were anesthetized and placed in sternal recumbancy on a positioning pad with stifles flexed and femora in contact with and perpendicular to the table-top. Hips were in a neutral position and bore a portion of the body weight. The percentage of the femoral head area covered by the dorsal rim of the acetabulum was calculated from the dorso-ventral radiographic projection.

Necropsy Evaluation and Tissue Collection

Subjects were euthanized at approximately 8 months by barbiturate overdose. The articular cartilage collection procedure has been described previously (2). Soft tissues were dissected and the joint capsule was excised. The joint was evaluated for macroscopic fibrillation of articular cartilage and capsular fibrosis, and volumes of synovial fluid and ligament of the femoral head were measured. Cartilage was collected from the superior perifoveal region of the femoral head characteristic for early lesion formation. The entire lesion was collected as a single sample if present. Cartilage was also collected from the concentric surrounding area.

Biochemical Assays

Biochemical assays were performed to detect the characteristic increase in water and fibronectin, and decrease in sulfated glycosaminoglycan (GAG) contents that precede macroscopic lesion formation (2,18). Cartilage samples were lyophilized and weighed. Water content was expressed as a percentage of the weight at collection.

Dimethylmethylene Blue Assay: GAG content was measured by dimethylmethylene blue assay (19). 1,9-dimethylmethylene blue (all chemicals: Sigma-Aldrich, St. Louis, MO, USA), a strongly metachromatic dye, was added to papain digested samples and the absorbance of the GAG-dye complex was measured at 535 nm on a spectrophotometer (Beckman Instruments, Inc., Fullerton, CA, USA). The standard was a serial dilution of chondroitin-4 sulfate.

Fibronectin ELISA: Fibronectin content was measured by enzyme linked immunosorbent assay (20). Urea extracted samples were assayed with a sandwich ELISA. The capture and detector antibodies were goat anti-human fibronectin (all

Table 1.2 Degeneration score assignment guidelines

Score	Necropsy Observation	Cartilage Biochemistry	
0	No abnormalities	Within normal range*	
1	Mild changes: ligament hypertrophy (volume < 1ml), mild capsular fibrosis, minimal effusion, no cartilage fibrillation	water increase GAG** decrease Fibronectin**	 < 5 % < 20 % < 600 ng/mg
2	Moderate changes: ligament hypertrophy (volume > 1ml), extensive capsular fibrosis, effusion, no cartilage fibrillation	water increase GAG decrease Fibronectin	> 5 % > 20 % > 600 ng/mg
3	Macroscopic lesion present		

* Reference values based on (2).
** Expressed per mg cartilage dry weight.

antibodies: ICN/Cappel, Aurora, OH, USA) and rabbit anti-human fibronectin, respectively. Antigen-detector antibody complexes were quantified using a peroxidase-linked goat anti-rabbit IgG antibody and an O-phenylenediamine substrate. Absorbance was measured at 490 nm with a reference wavelength of 630 nm on a microtitre plate reader (Tecan, Research Triangle Park, NC, USA). The standard was a serial dilution of purified plasma fibronectin.

Degeneration Score Assignment

A degeneration score of 0 to 3 was assigned to each hip based on cartilage biochemistry and necropsy examination (Table 1.2). Constituent values from the superior perifoveal area characteristic for lesion formation and the surrounding area were used for score assignment. Changes in gross joint structure characteristic of degeneration associated with DDH include capsular fibrosis, hypertrophy of the

femoral head ligament, effusion, and macroscopic cartilage fibrillation. Hips were scored independently by two of the authors (W.S.V.B.-F., R.J.T.). Discrepancies were reviewed and a score was reached by consensus.

Statistical Analyses

Data in this study occur in a natural hierarchical structure, with hips nested within dogs and dogs nested within litters. Observations are not independent, as hips within a dog are expected to be more similar than hips from different dogs, and dogs from the same litter are expected to be more similar than dogs from different litters. Hierarchical linear models (HLMs) explicitly address data dependency by using a sub-model for each level of the hierarchy; each submodel includes a level-specific error term (21).

A key feature of HLMs is that the total variance of the response variable is decomposed into components contributed by individual levels. A representative 2-level random effects model for the observed growth rate contained the grand mean, γ_{00}, a litter-level error (random) term u_{0j}, and a dog-within-litter error (random) term r_{ij}; the growth rate for dog *i* in litter *j*, λ_{ij}, was

$$\lambda_{ij} = \gamma_{00} + u_{0j} + r_{ij}\,.$$

Variance of the growth rate was

$$\mathrm{var}(\lambda_{ij}) = \mathrm{var}(u_{0j}) + \mathrm{var}(r_{ij}) = \sigma^2_{litter} + \sigma^2_{dog}\,.$$

Variance components were expressed as intraclass correlations, a measure of within-group similarity, for 2-level models (22) or as a percentage of the total variance for 3-level models. HLMs used included both fixed effects (phenotype, gender) and random effects (litter, dog within litter, hip within dog). See (23) for a review of effect classification in mixed models.

The 8-month hip degeneration score was an ordinal variable. A proportional odds model was used to estimate the effect of the independent variable on the log odds of a particular degeneration score (24). A typical model was

$$\text{logit}\left[P\left(score \le j\right)\right] = \alpha_j + \beta w, \quad j = 1,\ldots,J-1.$$

The model assumes that the effect of the independent variable body weight, *w*, is the same (proportional) for all degeneration score categories. The probability of a hip degeneration score indicating moderate biochemical changes (score 2) or lesion (score 3) was estimated from model results.

HLMs were implemented using the MIXED procedure in the SAS statistical software package (version 9.1, SAS Institute, Cary, NC). The restricted maximum likelihood procedure was used to estimate variance components. Degrees of freedom for F statistics were estimated using the Kenward-Roger approximation for unbalanced data (25). Estimated degrees of freedom are often fractional values. Proportional odds models were implemented using the LOGISTIC procedure in SAS. Rate of growth for the first three weeks of age was estimated using a simple exponential growth model ($w = w_0 e^{\lambda t}$). Strength of the linear relationship between body weight at successive ages and onset of ossification was estimated using ordinary least squares.

Statistical analysis consisted of three stages. First, the pattern of growth (body weight gain) for days 0-20 was examined. Next, the ability of the growth parameters to predict the age at ossification onset for the femoral capital epiphyses was investigated. Finally, the ability of the early growth parameters to predict outcomes of femoral head coverage and degeneration at early adulthood was investigated. *p*-values below 0.05 were considered statistically significant.

Results

Body Weight for 0-20 Days

Mean body weight at birth was 0.44 kg (SE 0.04). All pups were within two standard deviations of the colony mean (μ 0.43, σ 0.08 kg). Of the total variance in birth weight, 85.1% was due to among-litter differences and 14.9% to within-litter differences. Litter size was strongly associated with birth weight ($F(1, 2.77) = 39.37$, $p = 0.010$), accounting for 94.7% of the among-litter variance; pups from larger litters had lower birth weights. Birth weight for females was less than that for males (by 19.8 g); however, the difference was not significant ($F(1, 12.9) = 1.41$, $p = 0.256$) when controlling for litter size. There was no difference in birth weight between normal and dysplastic parental phenotypes ($F(1, 1.85) = 0.54$, $p = 0.543$) when controlling for litter size.

The body weight growth trajectory for the first 20 days was approximately exponential (Figure 1.3). Mean exponential growth rate (EGR) for body weight was 0.064 1/day (SE 0.004). EGR for females was less than that for males (by 0.007) ($F(1, 11.4) = 8.74$, $p = 0.013$) when controlling for birth weight. An intraclass correlation of 71.3% indicated the EGR was more similar within litters than among litters. Birth weight prediction of EGR approached conventional levels of significance ($F(1, 11.5) = 3.69$, $p = 0.080$), with lower birth weight subjects having a greater EGR. Inclusion of birth weight in the model reduced among-litter variance by 25.5% and within-litter variance by 20.1%. There was no difference in EGR between normal and dysplastic parental phenotypes ($F(1, 1.9) = 0.27$, $p = 0.657$). The percentage of the total variance in body weight explained by litter size decreased from 82.7% at day 0 (birth) to 32.8% at age 8

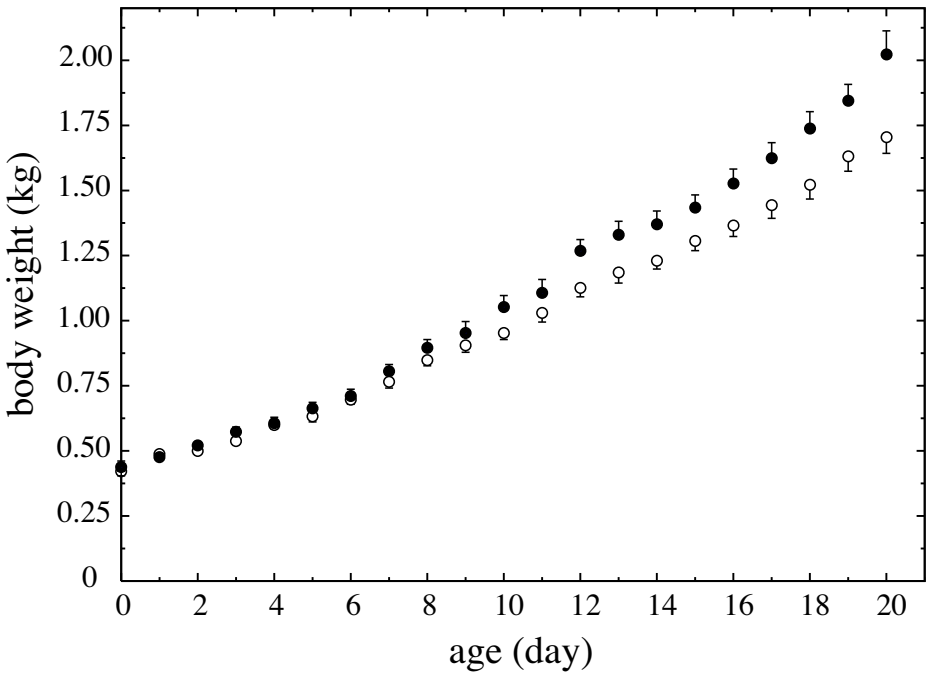

Figure 1.3 Body weight means for males (●) and females (○) from 0 to 20 days (n = 9 female, n = 8 male). Error bars represent SE.

days. By age 12 days, the association between litter size and body weight was no longer significant.

Age at Femoral Head Ossification Onset

Mean age at ossification onset was 12.12 days (SE 0.99). All pups were within two standard deviations of the colony mean (μ 12.69, σ 3.72 days). Of the total variance in age at ossification onset, 68.8% was due to among-litter differences, 23.4% to within-litter differences, and 7.8% to between-hip differences. Age at ossification onset was strongly associated with birth weight ($F(2, 30) = 38.27$, $p < 0.001$), with lower birth weight pups having a later age at onset. There was a significant interaction between parental phenotype and birth weight ($F(1, 12) = 5.14$, $p = 0.043$), with pups of normal parental phenotype having a slope of greater magnitude (Figure 1.4). Inclusion of the interaction in the model reduced the within-litter variance by 22.8%.

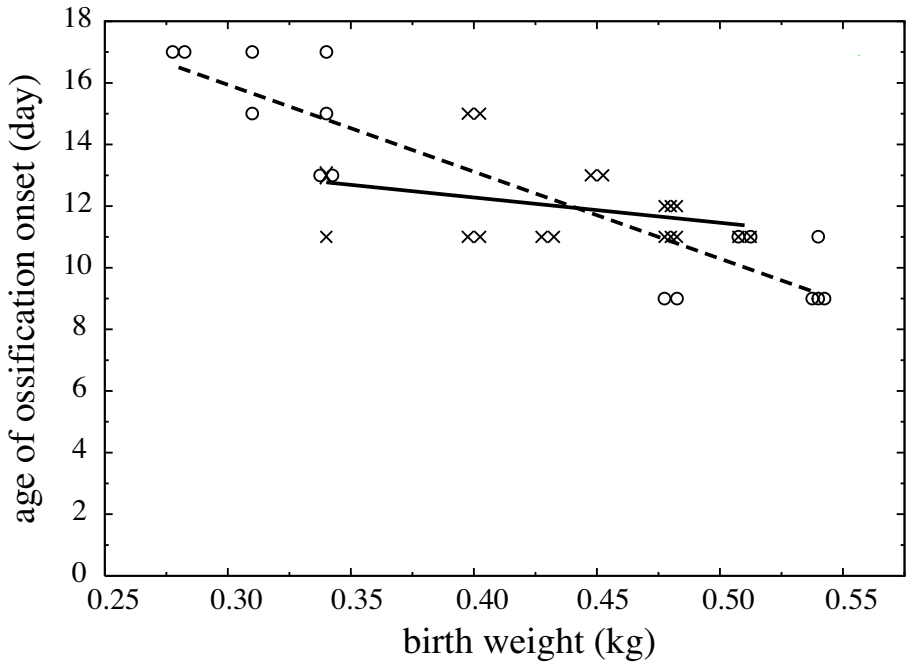

Figure 1.4 Age at femoral head ossification onset for pups from normal (○, ---) and dysplastic (×, —) parental phenotypes (n = 34 hips; n = 16 normal, n = 18 dysplastic phenotype). Coincident data points were moved by 0.0025 kg increments (Δ) to improve clarity (2 points: −Δ, +Δ; 3 points: −Δ, 0, +Δ).

The slope for the dysplastic parental phenotype was not significantly different from zero ($t(12) = -1.64$, $p = 0.126$). Ossification onset occurred 1.5 days earlier for females at the birth weight mean ($F(1, 12) = 9.43$, $p = 0.010$). The percentage of the total variance in age at ossification onset explained by body weight decreased rapidly from 65% at day 0 (birth) to 17% at age 8 days (Figure 1.5). (The strength of the initial relationship would persist if all subjects had identical growth rates.) Inclusion of body weight in the model did not reduce within-litter variance at any age before the age at ossification onset. Age at ossification onset was not significantly associated with the EGR ($F(1, 14) = 0.24$, $p = 0.632$).

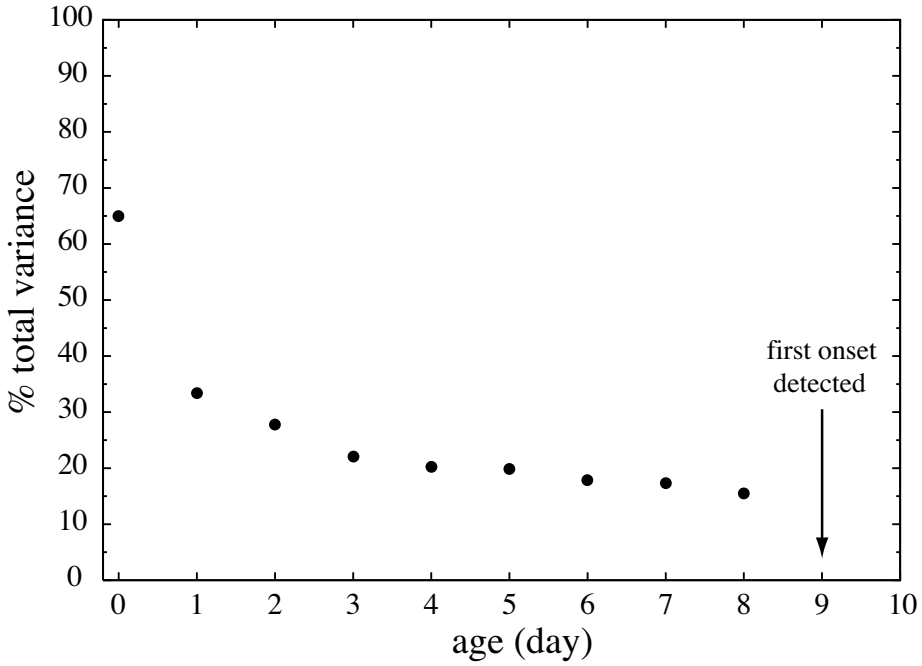

Figure 1.5 Percent of total variance for age at ossification onset explained by body weight for each age (n = 34 hips).

4-Month Femoral Head Coverage

Mean femoral head coverage was 64.0% (SE 1.9). No dislocations were detected radiographically or during physical exams. Femoral head coverage was associated with birth weight ($F(1, 15) = 6.59$, $p = 0.021$) and day 1 weight ($F(1, 15) = 4.59$, $p = 0.049$); lower weight subjects had greater femoral head coverage (Figure 1.6). Of the total variance in femoral head coverage, 4.5% was due to among-litter differences, 35.3% to within-litter differences, and 60.3% to between-hip differences. Inclusion of birth weight in the model reduced within-litter variance by 40.0% and accounted for all of the among-litter variance. Femoral head coverage was not associated with parental phenotype ($F(1, 3.12) = 0.00$, $p = 0.955$).

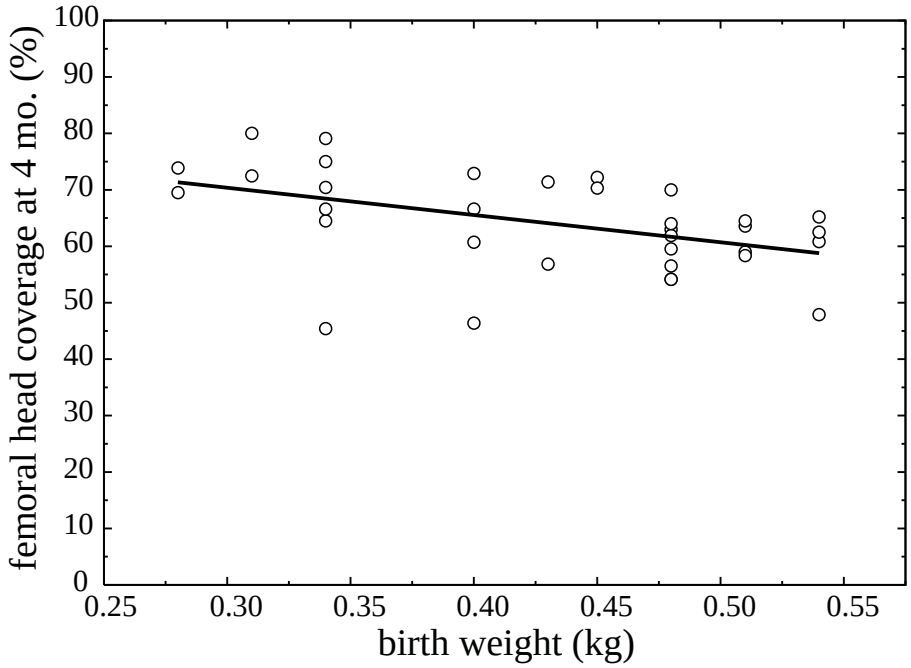

Figure 1.6 Femoral head coverage at 4 months as a function of birth weight (n = 34 hips). Solid line represents the hierarchical linear model.

8-Month Joint Degeneration Score

At 8 months, 9 hips had no abnormalities, 7 hips were mildly affected, 12 hips were moderately affected, and 6 hips had a macroscopic lesion (Table 1.3, Figure 1.7 example). Right and left hips were affected similarly with a maximum score difference of 1. The probability of moderate cartilage abnormality or lesion increased with increasing birth weight ($\chi^2 = 6.24$, $p = 0.013$) and was lower for females than for males ($\chi^2 = 4.08$, $p = 0.043$) (Figure 1.8). This probability increased with decreasing 4-month femoral head coverage ($\chi^2 = 11.93$, $p < 0.001$). The probability was not associated with parental phenotype ($\chi^2 = 0.51$, $p = 0.477$).

Discussion

Much research has focused on cartilage degeneration secondary to DDH (1,2,3); however, little is known about influences such as body weight on early postnatal hip

Table 1.3 Summary of cartilage extracellular matrix constituents and femoral head coverage by degeneration score group

Score	Water (%)	GAG* (μg/mg)	Fibronectin*† (ng/mg)	Femoral Head Coverage (%)
0 or 1	74.9 (0.77)	136.6 (6.99)	317.4 [251.4, 465.0]	68.1 (1.7)
2 or 3	78.1 (0.78)	115.5 (4.73)	958.4 [691.3, 1221.1]	60.5 (2.0)

* Expressed per mg tissue dry weight.
† Data summarized as median [1st, 3rd quartiles]; all other data summarized as mean (SE).

development. The objective of this initial study was to determine whether early postnatal body weight affected the course of hip development and joint health at adulthood in a canine model of DDH.

When studying early postnatal skeletal growth, prenatal growth and skeletal maturity at birth must be considered. Prenatal growth is the result of the interaction between the fetal genotype and the maternal intrauterine environment. One way in which the intrauterine environment influences growth is through a uterine size constraint during late gestation. The uterine size constraint results in a negative association between the number of fetuses and birth weight. This effect is seen in humans, where fetal weight for singletons and twins is similar until approximately 28 weeks, after which the rate of growth for twins slows relative to that of singletons (26). A similar effect is seen in mice, where the negative correlation of litter size and fetal weight does not begin until day 17.5 in a 19 day gestation (27). After birth, a period of accelerated, or catch-up, growth occurs (28). A negative association between litter size and birth weight was also found in this study. Lower birth weight pups had a greater EGR, indicating that

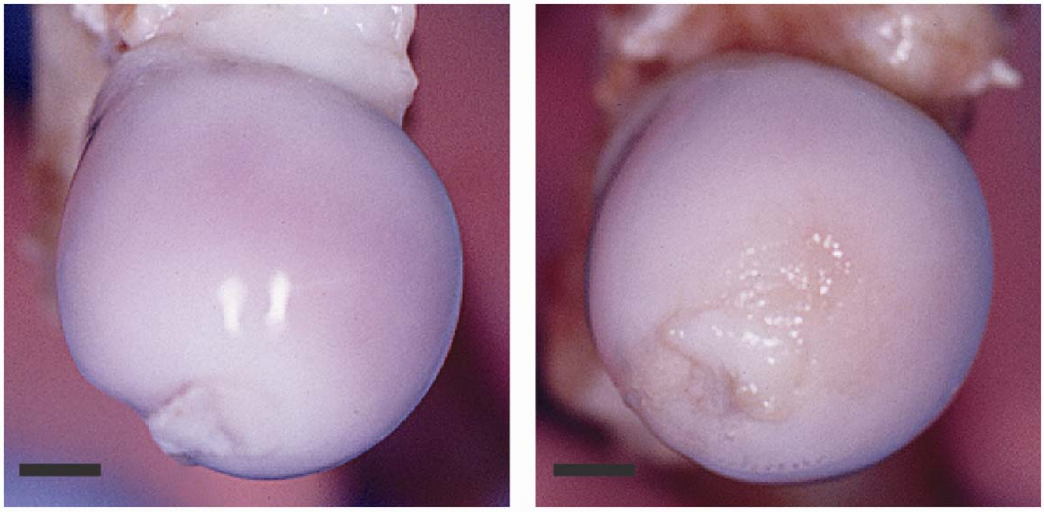

Figure 1.7 Articular surface for normal (L) and lesion (R) femoral heads. Note roughness in lesion example. Bar = 5 mm.

postnatal catch-up growth occurred. Intrauterine growth restriction was likely greater for larger litters.

If ossification rate is positively associated with volumetric growth rate, pups from larger litters would be skeletally less mature (proportionately less ossification) at birth than pups from smaller litters. There is little research addressing the relationship between birth weight and the extent of skeletal ossification. In late term pregnancy for rats (day 21), the extent of ossification in skeletal structures where ossification is beginning or still in progress is positively related to fetal weight (29). If this result in rats represents a general phenomenon of mammalian prenatal development, then the lower birth weight pups in the present study can be expected to have proportionately less ossification of the acetabulum and proximal femur at birth.

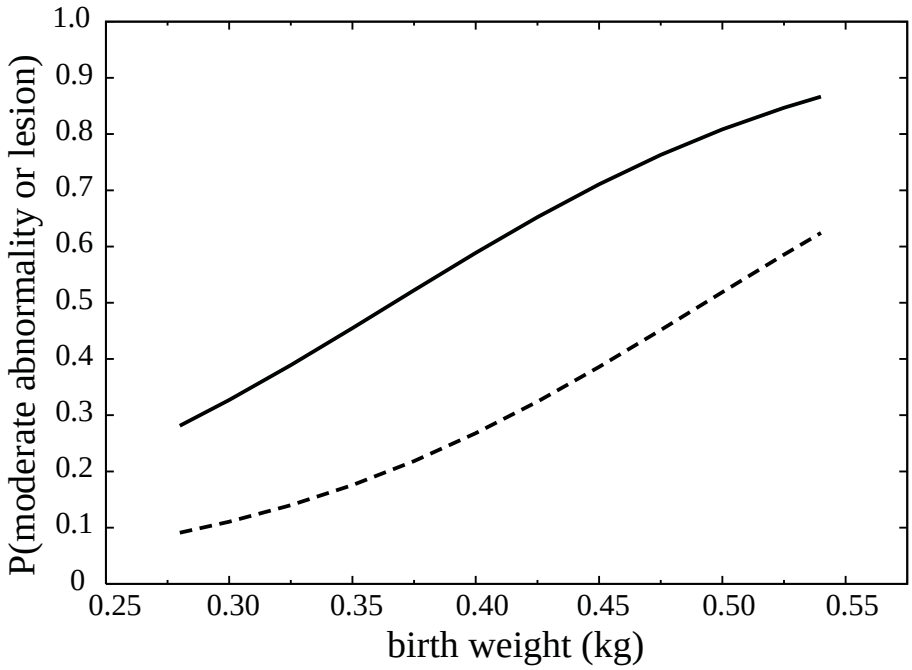

Figure 1.8 Probability of moderate abnormality or lesion of femoral head cartilage for males (—) and females (---) at 8 months (n = 9 female, n = 8 male).

Skeletal maturity at birth is also determined by length of gestation. Gestation length in litters of five or more pups has been shown to be shorter by 1.1 days than litters with fewer than 5 pups (30). Any decrease in length of gestation for larger litters would be a minor additive influence to the effects of late term growth rate reduction.

The age at ossification onset was significantly associated with birth weight; however, the variance attributed to body weight decayed rapidly with increasing age. This result is consistent with the degree of skeletal maturity at birth being the primary determinant of age at onset rather than body weight *per se*. Inclusion of body weight in the model did not reduce within-litter variance in age at ossification onset. A delay in skeletal maturity due to intrauterine crowding is a feature common to all pups within a litter. The remaining variance attributed to body weight at days 1 to 8 is likely due to the residual correlation between body weight and weight at birth.

The interpretation that degree of skeletal maturity at birth was the primary determinant of age at ossification onset does not imply that mechanical forces were not important for stimulating the onset of ossification. In clear cases of unilateral DDH, the onset and progression of ossification in the affected hip are delayed relative to the normal hip (31). The normal hip serves as a control for environmental and systemic factors, so the response due to differences in local mechanical environmental variables can be distinguished from other influences. This result supports the claim by Wilkinson (31) that a delay in the onset of ossification for the femoral epiphyses (up to age 12 months in human infants) was "of little consequence"; however, a unilateral retardation of ossification "might well suggest some pathological condition."

The interaction between birth weight and parental phenotype was significant when gender differences and birth weight were controlled. The magnitude of the slope for pups from dysplastic parental phenotype was less than the slope for pups from normal parental phenotype. The variance accounted for by the interaction was at the within-litter level. DDH in the Labrador retriever model is associated with greater hip joint laxity (9). If laxity is present at birth, the femoral head for pups with a dysplastic parental phenotype may be loaded in a more focal, eccentric fashion, thus altering the stimulus for ossification onset. Parental phenotype, however, was not predictive of 4-month femoral head coverage or 8-month degeneration score. The interpretation of an interaction for a small sample size should be made with considerable caution. Existence of this interaction must be confirmed in a larger sample.

Greater birth and day 1 weights were associated with reduced femoral head coverage at 4 months. Birth weight reduced the within-litter variance by 40.0%. Greater birth

weight may exceed the capacity of the immature connective tissues to maintain fully congruent articulation between the femoral head and the acetabulum. A subluxated femoral head will result in a smaller contact area and thus greater contact stresses on the dorsal-lateral margin of the acetabulum (32). This result suggests that birth weight was an important factor in establishing the manner in which the femoral head and acetabulum articulated, and as a result, influenced the development of acetabular depth.

The probability of moderate biochemical changes or lesion of the femoral head cartilage increased with increasing birth weight. The probability of degenerative changes for a given birth weight was lower for females than for males. There is no clear gender difference in DDH incidence for dogs as there is for humans (9). Persistence of a gender difference would be unlikely in a larger study population. The increased probability of degenerative changes with decreased femoral head coverage was similar to previous findings in Labrador retrievers (33). Degenerative changes were located in the characteristic superior perifoveal region of the femoral head that articulates with the dorsal rim of the acetabulum in subluxated hips (2). The degenerative changes are likely due to elevated contract stress that is a result of the focal, eccentric loading (34).

The lack of association between parental phenotype and 4-month femoral head coverage and 8-month degeneration score was likely due to the small sample size. Dysplastic progeny from phenotypically normal matings, and *vice versa*, are common. With this inheritance pattern, it is unlikely that parental phenotype will be strongly predictive of offspring phenotype in a small sample.

In conclusion, this study shows that increased early postnatal body weight, particularly birth weight, was associated with reduced femoral head coverage at 4 months and a greater probability of degenerative changes at 8 months. Increased birth weight was negatively associated with age at ossification onset for the femoral head; however, the effect was likely due to differences in skeletal maturity rather than to weight *per se*. These results support the hypothesis that increased body weight during the critical early postnatal period was sufficient to alter the course of hip development and result in measurable degenerative changes at adulthood.

Acknowledgments

The authors thank Alma Jo Williams for animal care and radiography, Margaret Vernier-Singer for assistance with tissue collection and biochemical assays, Liz Corey for performing the fibronectin ELISAs, and the Baker Institute for Animal Health, Cornell University, for access to the Labrador retriever breeding colony.

REFERENCES

1. Weinstein SL 1987 Natural history of congenital hip dislocation (CDH) and hip dysplasia. Clin Orthop 225:62-76

2. Burton-Wurster N, Farese JP, Todhunter RJ, Lust G 1999 Site-specific variation in femoral head cartilage composition in dogs at high and low risk for development of osteoarthritis: insights into cartilage degeneration. Osteoarthritis Cartilage 7:486-497

3. Jacobsen S, Honne-Holm S, Søballe K, Gebuhr P, Lund B 2005 Hip dysplasia and osteoarthritis a survery of 4151 subjects from the osteoarthrosis substudy of the Copenhagen city heart study. Acta Orthop Scand 76:149-158

4. Homer CJ, Baltz RD, Hickson GB, Miles PV, Newman TB, Shook JE, Zurhellen WM, Goldberg MJ, Harcke TH, Hirsch A, Lehmann H, Roy DR, Sunshine P 2000 Clinical practice guideline: early detection of developmental dysplasia of the hip. Pediatrics 105:896-905

5. Riser WH 1975 The dog as a model for the study of hip dysplasia. Vet Pathol 12:229-334

6. Cunningham FG, MacDonald PC, Gant NF 1989 Williams Obstetrics. Appleton & Lange, Norwalk, pp 177-180

7. Walker JM, Goldsmith CH 1981 Morphometric study of the fetal development of the human hip joint: significance for congenital hip disease. Yale J Biol Med 54:411-437

8. Breur GJ, Lust G, Todhunter RJ 2001 Genetics of canine hip dysplasia and other orthopaedic traits. In: Ruvinsky A, Sampson J (eds) The Genetics of the Dog. CABI Publishing, New York, pp 268-277

9. Lust G 1993 Other orthopedic diseases hip dysplasia in dogs. In: Slatter D (ed) Textbook of Small Animal Surgery. WB Saunders Company, Philadelphia, pp 1938-1944

10. Schoenecker PL, Lesker PA, Ogata K 1984 A dynamic model of experimental hip dysplasia – gross and histological pathology, and the effect of position of immobilization on capital femoral epiphyseal blood-flow. J Bone Joint Surg Am 66:1281-1288

11. Harrison TJ 1961 The influence of the femoral head on pelvic growth and acetabular form in the rat. J Anat 95:12-26

12. Coleman CR, Slager RF, Smith WS 1958 The effect of environmental influence on acetabular development. Surg Forum 9:775-780

13. Kealy RD, Olsson SE, Monti KL, Lawler DF, Biery DN, Helms RW, Lust G, Smith GK 1992 Effects of limited food consumption on the incidence of hip dysplasia in growing dogs. J Am Vet Med Assoc 201:857-863

14. Kealy RD, Lawler DF, Ballam JM, Lust G, Biery DN, Smith GK, Mantz SL 2000 Evaluation of the effect of limited food consumption on radiographic evidence of osteoarthritis in dogs. J Am Vet Med Assoc 217:1678-1680

15. Karlson EW, Mandl LA, Aweh GN, Sangha O, Miang MH, Grodstein F 2003 Total hip replacement due to osteoarthritis: the importance of age, obesity, and other modifiable risk factors. Am J Med 114:93-98

16. Todhunter RJ, Zachos TA, Gilbert RO, Erb HN, Williams AJ, Burton-Wurster N, Lust G 1997 Onset of epiphyseal mineralization and growth plate closure in radiographically normal and dysplastic Labrador Retrievers. J Am Vet Med Assoc 210:1458-1462

17. Farese JP, Todhunter RJ, Lust G, Williams AJ, Dykes NL 1998 Dorsolateral subluxation of hip joints in dogs measured in a weight-bearing position with radiography and computed tomography. Vet Surg 27:393-405

18. Mankin HJ, Brandt KD 1997 Pathogenesis of osteoarthritis. In: Kelley WN, Ruddy S, Harris ED, Sledge CB (eds) Textbook of Rheumatology. WB Saunders Company, Philadelphia, pp 1369-1382

19. Farndale RW, Sayers CA, Barrett AJ 1982 A direct spectrophotometric microassay for sulfated glycosaminoglycans in cartilage cultures. Connect Tissue Res 9:247-248

20. Wurster NB, Lust G 1982 Fibronectin in osteoarthritic canine articular cartilage. Biochem Biophys Res Commun 109:1094-1101

21. Raudenbush SW, Bryk AS 2002 Hierarchical linear models: applications and data analysis methods. Sage, Thousand Oaks, pp 228-251

22. Kuehl RO 2000 Design of experiments: statistical principles of research design and analysis. Duxbury, Pacific Grove, pp 148-169

23. Searle SR, Casella G, McCulloch CE 1992 Variance components. John Wiley & Sons, New York, pp 1-18

24. Agresti A 2002 Categorical data analysis. JohnWiley & Sons, Hoboken, pp 274-282

25. Littell RC 2003 Analysis of unbalanced mixed model data: a case study comparison of ANOVA versus REML/GLS. J Agric Biol Environ Stat 7:472-490

26. Snow MH 1986 Control of embryonic growth rate and fetal size in mammals. In: Faulkner F, Tanner JM (eds) Human Growth A Comprehensive Treatise. Plenum Press, New York, pp 67-82

27. Snow MH 1989 Embryonic growth and the experimental manipulation of fetal size. In: Tanner JM, Preece MA (eds) The Physiology of Human Growth. Cambridge University Press, Cambridge, pp 1-10

28. Harrison GA, Tanner JM, Pilbeam DR, Baker PT 1988 Human Biology. Oxford University Press, New York, pp 339-360

29. Chahoud I, Paumgartten FJR 2005 Relationships between fetal body weight of Wistar rats at term and the extent of skeletal ossification. Braz J Med Biol Res 38:565-575

30. Eilts BE, Davidson AP, Hosgood G, Paccamonti DL, Baker DG 2005 Factors affecting gestation duration in the bitch. Theriogenology 64:242-251

31. Wilkinson JA 1985 Congenital Displacement of the Hip Joint. Springer-Verlag, New York, pp 59-85

32. Pompe B, Daniel M, Sochor M, Vengust R, Kralj-Iglič V, Iglič A 2003 Gradient of contact stress in normal and dysplastic human hips. Med Eng Phys 25:379-385

33. Lust G, Williams AJ, Burton-Wurster N, Pijanowski GJ, Beck KA, Rubin G, Smith GK 1993 Joint laxity and its association with hip dysplasia in Labrador Retrievers. Am J Vet Res 54:1990-1999

34. Mavčič B, Pompe B, Antolič V, Daniel M, Iglič A, Kralj-Iglič V 2002 Mathematical estimation of stress distribution in normal and dysplastic human hips. J Orthop Res 20:1025-1030

CHAPTER 2

FEMORAL HEAD BONE MINERAL DENSITY PATTERNS ARE ALTERED BY SUBLUXATION DURING DEVEOPMENT IN A CANINE MODEL OF DDH

Abstract

Developmental dysplasia of the hip (DDH) is a frequent cause of early onset osteoarthritis; however, little is known about the effect of altered articulation on the postnatal development of the hip. The objectives of this research were to quantify the evolving bone mineral density (BMD) distribution of the femoral head secondary center of ossification (SCO), and to test for associations between BMD distribution, hip subluxation, and joint degeneration. Serial quantitative computed tomography was used to measure BMD noninvasively in a canine model of DDH. Twenty-eight hips in 14 dogs were scanned at 7 ages from 4 weeks to early skeletal maturity at 32 weeks. During SCO volumetric and body weight growth acceleration, there was little change in BMD. After growth deceleration, BMD increased rapidly and local high density regions became apparent. Greater subluxation was associated with lower early mean SCO density, and, at 32 weeks, with greater profile peak density and greater area of high density subchondral bone in a more lateral location. Subluxation was also associated with a greater probability of degenerative changes at 32 weeks. Differences in high density bone were found primarily in the subchondral region, with more subtle differences occurring proximal to the growth plate. Density differences at 32 weeks were typically not detectable at 14 weeks. Measures of BMD distribution adaptation to the focal, eccentric loading of subluxation may provide a basis for assessing *in vivo* function during development and identifying hips at risk of early onset osteoarthritis secondary to DDH.

Introduction

Developmental dysplasia of the hip (DDH) is characterized in the adult by joint laxity and subluxation, and malformation of the femoral head and acetabulum. Joint subluxation and malformation cause a chronic, focal overload of the articular cartilage, inevitably resulting in the early onset of osteoarthritis (OA) (1-4) (Figure 2.1). In the neonate, DDH is predominantly characterized by laxity, ranging from mild subluxation to complete dislocation. The incidence of DDH reported for neonates ranges from 1.5 to 20 per 1000 births (5), with as many as 1 in 100 exhibiting evidence of hip instability at birth (6). A recent literature survey reported that the majority of hips with instability at birth were diagnosed as normal at follow-up examinations (>60% for clinical examination and >90% for ultrasound examination) (5). An assessment of hip health at adulthood is generally not available for infants evaluated in screening studies because poor functional outcomes due to OA may not be evident for decades, even with early onset. For idiopathic hip OA, 20% to 50% of the cases have been attributed to subluxation or acetabular dysplasia (4), suggesting that the population incidence of DDH may be much higher than screening studies indicate.

Little is known about the effect of chronic overload due to subluxation on the course of early postnatal hip development. At birth, for humans and most other mammals, the majority of the femoral diaphysis has ossified while the proximal femur is still composed of cartilage. The cartilage is replaced by bone through the advancement of the primary ossification front and the initiation of secondary centers of ossification (SCO). The SCO of the femoral head grows, through the process of endochondral ossification, to form the portion of the femoral head that articulates with the

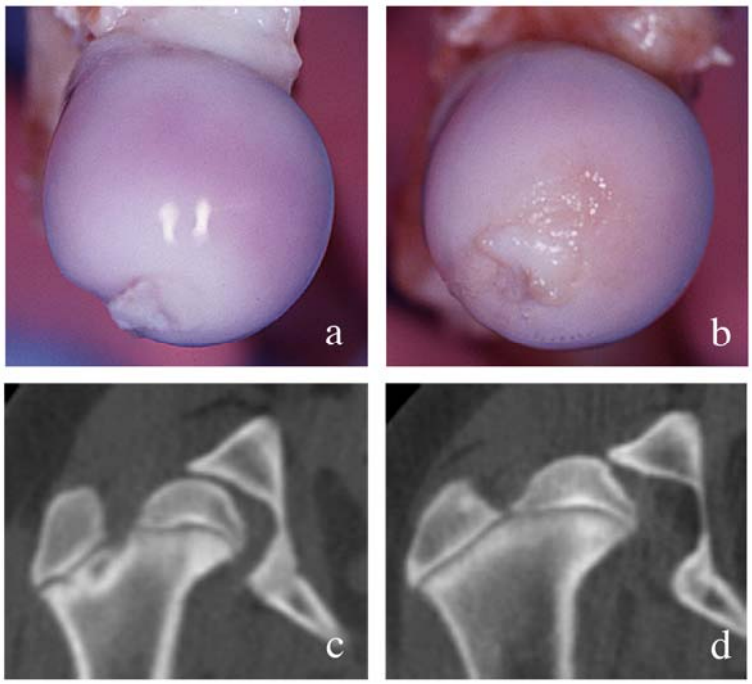

Figure 2.1 Articular surface of canine femoral heads at necropsy (a, b) with corresponding 32-week QCT images (c, d) for normal (a, c) and lesion (b, d) examples. Note cartilage roughness and focal, eccentric loading due to subluxation in lesion example.

acetabulum. Bone can be regarded as a self-organizing system with properties that emerge in response to persistent environmental stimuli (7). Modeling and remodeling during growth produce skeletal structures that are mechanically adapted to the local loading environment (8, review). Modeling results in site-specific alterations of architecture when mechanical loading changes, including altered patterns of bone mineral deposition and altered shape. The relationship between bone mineral density (BMD) and measures of bone material properties and overall strength has been demonstrated for mature and immature bone (9-11). The focus of this research was to measure the pattern of BMD established during development, and to test for pattern differences due to subluxation characteristic of DDH.

Three density structures clearly recognizable in cut sections and in computed tomography images have been described for the mature human femoral head: 1) an epiphyseal scar with a high-density central region, 2) a subchondral shell, and 3) higher density cancellous bone connecting the subchondral shell and epiphyseal scar (12,13). Similar structures have been observed in the canine femoral head (14,15). Little is known about the emergence of these density structures during development, or the extent to which focal, eccentric loading in subluxated hips alters the emerging BMD pattern.

Hips appearing to have normal conformation on plain radiographs have had elevated cartilage contact pressure demonstrated in 3-dimensional finite element models (1). Although the radiograph is a common hip assessment tool, it does not provide an adequate basis for detailed evaluation of bone structure. Spatial BMD distribution and subtle shape differences for mild to moderate DDH may not be apparent in a 2-dimensional projection of a 3-dimensional structure. Measures of femoral head BMD distribution would reflect adaptation to *in vivo* loading patterns, and would serve as a more sensitive, and much needed, measure of functional outcome, prior to the onset of OA (5).

The objectives of this study were to quantify the statistical and spatial distribution patterns of femoral head SCO BMD accrual during development and to test the association of BMD measures with hip subluxation and degeneration measures. The dog, a naturally occurring model of OA onset secondary to DDH, was used. The dog model has been previously described, and it shares many of the characteristic morphological and biochemical features of DDH in humans (4,16,17). *In vivo* BMD of the femoral head SCO was noninvasively estimated using serial quantitative

computed tomography (QCT) during postnatal growth. Degeneration status of the hip was assessed at early skeletal maturity. We hypothesized that bony adaptation to chronic subluxation would be manifested as 1) a local density increase at the site of load application, with an overall decrease in SCO mean density, 2) an increase in size of the high density region associated with the articular surface, and 3) a change in medial-lateral location of the high density region associated with the articular surface. Measures of the emerging BMD patterns should reflect adaptation to *in vivo* hip function and may provide a basis for identifying hips at risk of early onset OA.

Methods

Experimental Design

The BMD distribution within the femoral head SCO was characterized non-invasively during postnatal development using serial QCT. A longitudinal design was chosen to quantify patterns of intra-individual BMD change with age, and to evaluate the association of inter-individual BMD differences with subluxation and degeneration measures. Scan ages for BMD evaluation were approximately 4, 6, 8, 10, 14, 24, and 32 weeks. Body weight was measured at each scan acquisition. The statistical distribution of the calibrated QCT image voxels was characterized for each SCO at each age; spatial distribution was characterized at 14 and 32 weeks. The presence of hip joint degeneration was assessed at early skeletal maturity, approximately 32 weeks. The associations between features of BMD distribution, joint subluxation, and degeneration status were examined.

Animals

A sample of 17 Labrador retrievers, previously described (18), was obtained from a colony maintained by the Baker Institute for Animal Health, Cornell University. Two

to 4 dogs were randomly selected from the first 5 available litters. The phenotype of both sire and dam was either normal or dysplastic. The pattern of inheritance for hip morphology is complex; dysplastic offspring from phenotypically normal parents, and *vice versa*, are common. Fourteen of the 17 Labradors had quantitative computed tomography (QCT) scans with a calibration standard at each acquisition and were included in this study. This sample included 6 females and 8 males. Two dogs were not scanned at 24 weeks, an age that was not the focus of BMD spatial distribution analyses. This study was approved by the Cornell University Institutional Animal Care and Use Committee.

Radiography for Femoral Head Coverage

The dorso-lateral subluxation procedure (19,20) was used to measure femoral head coverage at approximately 16 and 32 weeks. Dogs were anesthetized and placed in sternal recumbancy on a positioning pad with stifles flexed and femora perpendicular to the table-top. The dorso-ventral radiographic projection was used to calculate the percentage of the femoral head area covered by the dorsal rim of the acetabulum. Femoral head coverage is strongly associated with development of OA secondary to DDH (21).

QCT Image Acquisition

QCT images of the hip joint were acquired in axial mode with an x-ray tube voltage and current of 130 kVp and 125 mA, respectively (PQS, Picker International, Inc., Cleveland, Ohio). The temporal scan series had 1 mm thick contiguous slices, with in-plane resolution ranging from 0.35×0.35 mm at 4 weeks to 0.78×0.78 mm at 32 weeks. The standard image reconstruction algorithm with an image matrix size of

512×512 voxels was used. Dogs were heavily sedated and placed in the same position used for the dorso-lateral subluxation procedure.

A calibration standard was placed on the dorsum above the hips and was scanned simultaneously. The standard provided a consistent intra- and inter-subject basis for BMD estimation and comparison over the course of the study. The standard consisted of three 2.5 cm diameter rods of calcium hydroxyapatite, $Ca_{10}(PO_4)_6(OH)_2$, in water-equivalent epoxy resin (Computerized Imaging Reference Systems, Inc., Norfolk, VA) with mineral concentrations of 400, 800, and 1200 mg/cm^3.

Hip Joint Degeneration Score Assignment

At the conclusion of the study, at age approximately 32 weeks, each hip was evaluated via necropsy and articular cartilage matrix component assays, and a degeneration score was assigned. Tissue collection, analysis, and score assignment have been described in detail previously (18). Joints were evaluated for gross changes characteristic of DDH associated degeneration, including capsule fibrosis, hypertrophy of the femoral head ligament, effusion, and macroscopic cartilage fibrillation. Biochemical assays of the superior perifoveal and surrounding cartilage were performed to detect the characteristic increase in water and fibronectin and the decrease in sulfated glycosaminoglycan contents that precede macroscopic lesion formation. Each hip was assigned an ordinal degeneration score of 0 to 3, with 0 representing no abnormalities and 3 representing a macroscopic lesion (Table 2.1).

QCT Image Processing

Preprocessing: Random noise was reduced by applying a 3×3 median filter (22). Images were resampled to an isotropic voxel dimension of 0.25 mm using trilinear

Table 2.1 Summary of degeneration scores for SCOs included in the BMD analysis sample

Score	Degeneration Status	Number of Hips
0	No abnormalities	8
1	Mild changes	6
2	Moderate changes	8
3	Macroscopic lesion present	6

interpolation. Image super-sampling provided a smoother representation of the SCO surface and facilitated segmentation of the SCO from the proximal femoral neck. The VisionX computer vision system (www.via.cornell.edu/visionx) was used as the basis for image processing operations.

BMD Calibration: Image calibration was performed to convert bone voxel x-ray attenuation values to *in vivo* BMD estimates. The spatial location of each standard rod within the images was determined using a binary mask image and the mutual information matching metric (23). Mutual information for two images A and B is defined as

$$I(A,B) = \sum_{a,b} p_{AB}(a,b) \log \frac{p_{AB}(a,b)}{p_A(a) \cdot p_B(b)}$$

where $p_A(a)$ and $p_B(b)$ are the marginal probability distributions and $p_{AB}(a,b)$ is the joint probability distribution. Mutual information measures the distance between the joint distribution and complete independence, where $p_{AB}(a,b) = p_A(a) \cdot p_B(b)$, and is maximized at geometric alignment of corresponding features. The linear calibration equation was generated by least squares regression of the mean voxel attenuation

values and the known mineral concentrations. The calibration equation was generated using only those images in which the SCO was present. The minimum estimated BMD for SCOs was approximately 125 mg/cm^3, below the minimum standard concentration. The x-ray attenuation coefficient is a linear function of material density (24); however, calibrated bone mineral densities below the standard range may be less accurate than if the standard had spanned the complete range of expected density values.

SCO Segmentation: SCOs were segmented from the surrounding tissue using a binary image mask. The mask was generated with a simple threshold of 125 mg/cm^3 at the early ages or with iterative region growing at advanced ossification. High density seed regions were created by increasing the threshold until the SCO was separated from the femoral neck in all images. The seed regions were then iteratively grown, within a boundary constraint of the 125 mg/cm^3 threshold, until there was no further increase in size. Connected component labeling was used to select the SCO. Manual intervention was occasionally required at advanced ossification to separate the SCO in regions of high growth plate curvature. Discretization of the continuous x-ray attenuation field results in boundary voxels that represent more than one tissue type. These partial volume voxels were defined to be any boundary voxel with a density value below the 2.5th percentile of the density distribution. All voxels fulfilling these requirements were stripped from the SCO boundary. A morphological opening was performed to remove any spurious boundary irregularities. Volume of the segmented SCO was recorded.

SCO Orientation Standardization: SCOs were placed in a standard orientation with respect to the image Cartesian coordinate axes using geometric moments (25,26). For

3-dimensional isotropic images of size $M \times N \times L$, moments $\{m_{pqr}\}$ of order n, where $n = p + q + r$, are defined as:

$$m_{pqr} = \sum_{x=0}^{M-1} \sum_{y=0}^{N-1} \sum_{z=0}^{L-1} x^p y^q z^r v(x, y, z)$$

where the voxel values for binary images are $\{0,1\}$ with voxels representing the SCO having a value of 1. The location of the centroid $(\bar{x}, \bar{y}, \bar{z})$ is defined as

$$\bar{x} = \frac{m_{100}}{m_{000}} \qquad \bar{y} = \frac{m_{010}}{m_{000}} \qquad \bar{z} = \frac{m_{001}}{m_{000}}.$$

The centroid of the SCO was translated to coincide with the origin of the image coordinate system. The principal axes were computed by solving the eigenvalue equation $Mx = \lambda x$ for the second order moments where

$$M = \begin{bmatrix} m_{200} & m_{110} & m_{101} \\ m_{110} & m_{020} & m_{011} \\ m_{101} & m_{011} & m_{002} \end{bmatrix}.$$

The eigenvalues are the roots of the characteristic equation, $|M - \lambda I| = 0$, and represent the moments of inertia about the principal axes (eigenvectors). The SCO principal axes were aligned with the image coordinate axes via rigid body rotation: the major principal axis (largest eigenvalue) was aligned with the x-axis, the 2nd principal axis (2nd largest eigenvalue) was aligned with the y-axis, and the minor principal axis (smallest eigenvalue) was aligned with the z-axis. The SCO was not rotationally symmetric at any point during the evaluation period. Finally, the anatomical handedness of the SCO was standardized using a reflection operation. The left hip was chosen as the default and the right hip was reflected in the sagittal plane.

Body Weight and SCO Volumetric Growth Curves

Growth curves were fitted to individual body weight and SCO volume data records. The Janoschek curve (27), a smooth, monotonically increasing function, was used. The equation, shown parametrized for body weight, was

$$w(t) = w_f - (w_f - w_0)e^{-kt^p}$$

where w_0 was the weight at t_0, w_f was the asymptotic adult weight, *k* was a constant, and p was a shape parameter. The growth curve was fitted to the average of the right and left SCO volumes. The nonlinear regression procedure, NLIN, in the SAS statistical software package (version 9.1, SAS Institute, Cary, NC) was used to estimate the parameter values. A pseudo-R^2 statistic was used to evaluate the growth curve's goodness of fit (28). The pseudo-R^2 statistic is a function of the residual and corrected total sums of squares, $SS_{residual}$ and SS_{total} respectively, where

$$Pseudo R^2 = 1 - \frac{SS_{residual}}{SS_{total}}.$$

The Janoschek growth curve provided a good fit to the data with a minimum pseudo-R^2 of 0.996 for SCO volume and 0.997 for body weight. The curve fits were used as an analytical tool to track growth and estimate the age at which the maximum growth rate (point of inflection) occurred.

BMD Statistical Distribution and Mean Temporal Trajectory

The statistical distribution of the calibrated voxel BMD values was characterized for each QCT scan of each SCO. The central tendency was represented by the mean and median, the range was represented by the 3rd and 97th percentiles, and the central 50% of the distribution was given by the difference between the 25th and 75th percentiles. Box plots were constructed for visual representation.

The mean BMD was approximately constant between 28 and 98 days, and exhibited a positive slope after 98 days. This temporal trend was modeled using a piecewise linear spline function with first order continuity and a single knot (29). The spline was

a linear combination of 3 basis functions: 1, t, and $(t-\kappa)_+$, where κ specified the knot location. The spline model was parameterized for fitting as:

$$d_i = \begin{cases} \beta_0 + S_1 t_i, & t_i \le \kappa \\ \beta_0 + S_1\kappa + S_2(t_i - \kappa)_+, & t_i > \kappa \end{cases} \quad \text{where} \quad (a)_+ \equiv \begin{cases} 0, & a \le 0 \\ a, & a > 0 \end{cases}$$

where β_0 was the intercept, and S_1 and S_2 were the pre- and post-knot slopes, respectively. Polynomial coefficients and the knot location were estimated for individual SCO mean BMD trajectories with the nonlinear regression procedure, NLIN, in the SAS statistical software package, using the Marquardt iterative method. The grand mean of the pre-knot slope was not significantly different from zero; therefore, a reduced, 3-parameter model was fitted. Descriptive statistics were calculated to summarize the individual model parameters. Associations of the model parameters with femoral head coverage and degeneration score were tested using hierarchical linear models and proportional odds models, respectively.

The nonlinear regression convergence criterion was not met for 3 SCOs when fitting the full model, and for 1 SCO when fitting the reduced model. The parameters for the nonconverged full models were excluded from all calculations. For the reduced model, the minimization had identified a finite minimum region rather than a minimum point. Similar parameter estimates ($\le 0.34\%$ difference) were generated using different starting points and iterative methods (Gauss, Newton). The model parameters were included in all subsequent calculations.

Spherical BMD Projections

Size-normalized spherical projections of selected BMD values were generated to evaluate the high density regions associated with the articular surface and capital femoral growth plate. The maximum BMD was selected from a region-specific search

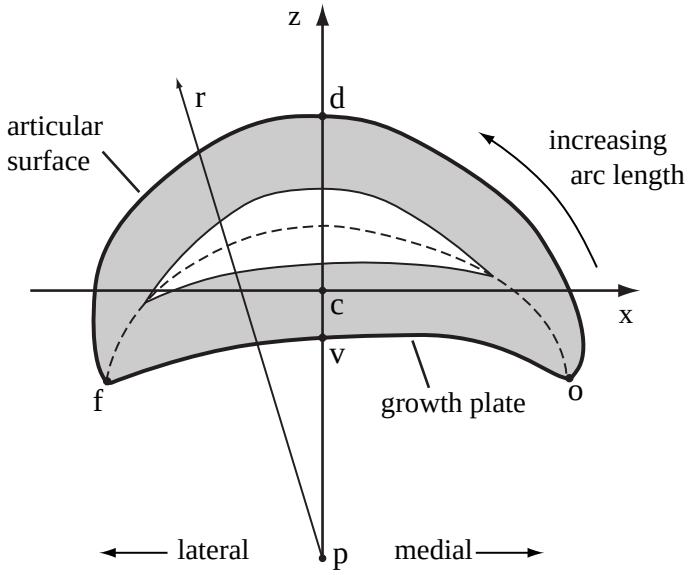

Figure 2.2 2D schematic of BMD projection method. The outline represents an SCO cross section. The vertical and horizontal lines represent the principal axes passing through the centroid (c). The sample ray (r) originates at the projection point (p). The search area for the regional maximum BMD values is shaded. The dorso-ventral thickness is the distance along the principal axis (z) between the most dorsal (d) and ventral (v) points. Mid-point density was sampled along the dashed line. The normalized arc length measure was 0 at the most medial point (o) and 100 at the most lateral point (f).

space (Figure 2.2). The projection point was located below the ventral surface of the SCO at a distance equal to the dorso-ventral thickness at the centroid. A unit sphere, tessellated with triangular polygons, was centered at the projection point. To tessellate the unit sphere, each face of an inscribed icosahedron was subdivided into smaller triangular polygons and the vertices were projected to the surface of the sphere (30). The direction of each sampling ray was determined by the projection point and a vertex on the sphere. BMD along each ray with nonzero values was sampled at intervals equal to half of the voxel dimension using tri-linear interpolation. The BMD assigned to each polygon was the average of the 3 vertex values. Division of each icosahedron edge by 100 yielded 100,000 polygons for the unit hemisphere.

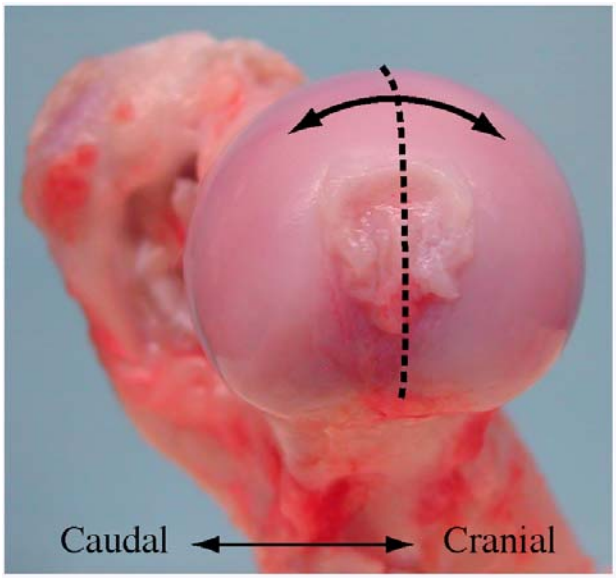

Figure 2.3 Medial-to-lateral view of a left femoral head. The solid line indicates the path of articulation. The dashed line indicates the approximate location of the BMD profile. The femur is positioned in the approximate neutral stance.

The search space for the maximum BMD was defined as a distance equal to one third of the dorso-ventral thickness from the corresponding surface along the sample ray (Figure 2.2). Near the margins, where the total thickness was less than two thirds of the dorso-ventral thickness, the array of sampled values was divided into two equal search spaces. The maximum value was assigned to the corresponding polygon on the unit sphere. Separate projections were formed for the articular and growth plate regions; BMD at the mid-point was also projected. Projections were generated for SCOs at 14 and 32 weeks. Regions were defined as high density if the BMD was $\geq 90^{th}$ percentile for that SCO. The proportion of the area designated as high density was recorded.

Medial-Lateral BMD Profile Sampling

The medial-lateral location (MLL) of the high BMD regions was measured using a 1-dimensional sample (profile) of each projection. A sampling plane was passed

through the articular perifoveal region, characteristic for lesion formation, and oriented approximately parallel to the frontal plane (Figure 2.3). The orientation of each plane was adjusted to enforce passage through the location of greatest BMD in the articular perifoveal region. The same plane orientation was used to sample each of the three projections. The BMD of all polygons intersecting the plane was sampled. The arc length along the circle formed by the intersection of the unit projection hemisphere and the plane was recorded as the BMD sample location (Figure 2.2). The arc length was standardized to a scale of 0 to 100 to represent the relative location and was expressed as a percentage.

Functional Data Analysis of Medial-Lateral BMD Profiles

The medial-lateral BMD profiles were evaluated using a functional data analysis approach. See (31) for an exposition of this approach. Functional data analysis treats the entire curve as the unit of analysis rather than as a collection of individual data points. BMD as a continuous function of normalized arc length was estimated by fitting the individual data records with a B-spline. The total number of spline basis functions $B_k(a,\alpha)$ was determined by the order *m* of the polynomial and the number of data intervals *L* of the knot sequence α, less one, where

$$d_j(a) = \sum_{k=1}^{m+L-1} c_{jk} B_k(a,\alpha).$$

The basis function coefficients c_{jk} were estimated using least squares approximation. A polynomial of order 6 (degree 5) and a knot sequence defining 14 equal arc length intervals were used. See (32,33) for B-spline formulation. The mean and standard deviation for the fitted BMD profiles were summarized using point-by-point analogues of the univariate measures where

$$\bar{d}(a) = N^{-1}\sum_{j=1}^{N} d_j(a) \quad \text{and} \quad \hat{\sigma} = \left[(N-1)^{-1}\sum_{j=1}^{N}\left[d_j(a) - \bar{d}(a) \right]^2 \right]^{\frac{1}{2}}.$$

The peak of the BMD function for the articular and growth plate profiles was located by sampling at normalized arc length increments of 0.01. The magnitude and MLL of the profile peak were recorded. For each SCO, the ratio of the articular and growth plate peak magnitudes was calculated. Associations of peak MLL and magnitude with femoral head coverage and degeneration score were tested using hierarchical linear models and proportional odds models, respectively.

The variance of the BMD profile shape for the articular and growth plate regions was evaluated using principal component analysis (PCA) for functional data (31). The PC weight functions calculated for functional PCAs are analogous to the PC weight values of the more familiar multivariate PCA. A roughness penalty was added to the least squares fitting criterion to remove extraneous variance. Curvature is often represented by the second derivative of a function, with roughness defined as the integral of the curvature (31). For each BMD data record $\mathbf{y}_j$, the roughness of the spline first derivative was penalized:

$$PENSSE = SSE(\mathbf{y}_j, \mathbf{c}_j) + \lambda \int d_j'''(a)\, da\,.$$

A weight of $\lambda = 500$ removed minor undulations while retaining the overall curve shape.

The covariance function, an analogue of the covariance matrix for multivariate data, was expressed over all possible combinations of arc length (a_1, a_2):

$$\upsilon(a_1, a_2) = (N_S - 1)^{-1} \sum_{j=1}^{N_S} \left\{ d_j(a_1) - \bar{d}(a_1) \right\} \left\{ d_j(a_2) - \bar{d}(a_2) \right\}$$

where N_S is the number of SCOs. See (34) for a review of multivariate PCA, and (31) for the extension of PCA to functional data. The PC weights $\xi_m(s)$ are functions that satisfy the equation

$$\int \upsilon(s,t)\xi_m(t)dt = \rho_m\xi_m(s)$$

where ρ_m are the eigenvalues.

The PC scores, f_{jm}, for the functional data $d_j(s)$ (coefficients for the PC basis expansion) are expressed as

$$f_{jm} = \int \xi_m(s)d_j(s)\,ds \quad j = 1\ldots N_S, m = 1\ldots N_{PC}$$

where N_{PC} is the number of PC retained for the new basis. The first 4 PCs accounted for greater than 90% of the total variance and were retained as the new orthogonal basis for expanding the density functions. A VARIMAX rotation was applied to the 4 retained PCs to improve interpretation of the modes of variance. The VARIMAX criterion selects the rotation that maximizes the variance of the squared PC weights for the new orthonormal basis, and thus increases the clustering of information (34). The rotated PC weight functions were plotted as perturbations of the mean density function $\bar{d}(a) \pm 1 s_m \xi_m(a)$ where s_m is the sample standard deviation for the m^{th} principal component. Associations of PC scores with femoral head coverage and degeneration score were tested using hierarchical linear models and proportional odds models, respectively. Matlab (The MathWorks, Inc., Natick, MA) functions used to carry out the B-spline fits and PCA were available from the authors of (31) at http://www.functionaldata.org.

Statistical Analyses

Data in this study occur in a natural hierarchical structure, with hips nested within dogs and dogs nested within litters. Observations are not independent, as hips within a

dog are expected to be more similar than hips from different dogs, and dogs from the same litter are expected to be more similar than dogs from different litters. Hierarchical linear models (HLMs) explicitly address data dependency by using a sub-model for each level of the hierarchy; each submodel includes a level-specific error term (35).

A key feature of HLMs is that the total variance of the response variable is partitioned into portions contributed by individual levels. An unconditional 3-level random effects model contains a grand mean γ_{000} and 3 random error terms: u_{00k} for litter-level error, r_{0jk} for dog-within-litter error, and e_{ijk} for hip-within-dog error. The model for dependent variable λ_{ijk} (*e.g.* profile peak magnitude) for hip *i* in dog *j* in litter *k* was

$$\lambda_{ijk} = \gamma_{000} + u_{00k} + r_{0jk} + e_{ijk}$$

where the variance was

$$\text{var}(\lambda_{ijk}) = \text{var}(u_{00k}) + \text{var}(r_{0jk}) + \text{var}(e_{ijk}) = \sigma^2_{litter} + \sigma^2_{dog} + \sigma^2_{hip}\,.$$

HLMs used here included both fixed effects (body weight, gender) and random effects (litter, dog within litter, hip within dog). See (36) for a review of effect classification in mixed models.

The 32-week hip degeneration score was an ordinal variable. A proportional odds model was used to estimate the effect of the independent variable on the log odds of a particular degeneration score (37). A typical model was

$$\text{logit}\left[P\left(score \le j\right)\right] = \alpha_j + \beta x, \quad j = 1,\ldots,J-1\,.$$

The model assumes that the effect of the independent variable femoral head coverage, *x*, is the same (proportional) for all degeneration score categories. The χ^2 test statistic for the slope coefficient β (1 degree of freedom) was reported.

HLMs were implemented using the MIXED procedure in the SAS statistical software package (version 9.1, SAS Institute, Cary, NC). The variance partition was estimated using the restricted maximum likelihood procedure. Degrees of freedom for *F* statistics were estimated using the Kenward-Roger approximation for unbalanced data (38). Estimated degrees of freedom are often fractional values and are determined by the degree of data dependency. Proportional odds models were implemented using the LOGISTIC procedure in SAS. *p*-values below 0.05 were considered statistically significant. All *t*-tests were 2-tailed unless the alternative hypothesis was one-directional, which required 1-tailed *t*-tests.

The sample size for this study was necessarily small because of the high cost per dog of the project's longitudinal design and complex measurements. The study was exploratory by design, due to the absence of previous research on the issues addressed here. *p*-values below 0.05 were considered statistically significant. Because of the small sample size and the exploratory nature of this study, *p*-values between 0.05 and 0.10 were considered suggestive of significance; variables with such *p*-values should be investigated further in more extensive future studies.

Results

The mature size of the SCO was attained by 32 weeks; the capital femoral growth plate had narrowed and bony bridging had begun in isolated regions. The 32 week volume was 3.4 cm^3 (SD 0.7). The size of the SCO at 4 weeks was 4.8% (SD 2.5) of the final volume. No growth disturbance due to injury or systemic disease was observed.

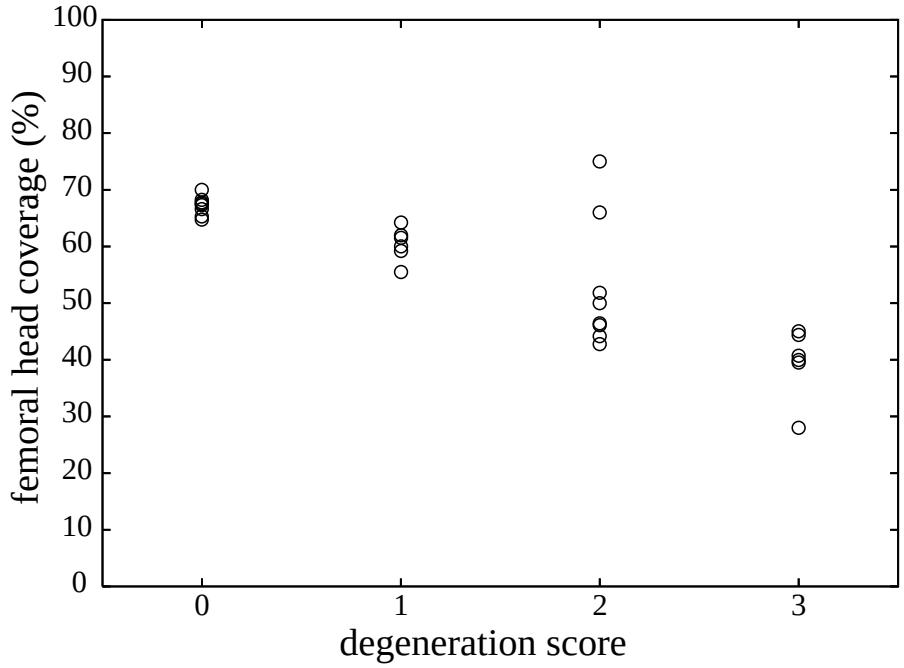

Figure 2.4 Femoral head coverage at 32 weeks by degeneration score. The hips from 1 dog produced the 2 outlying points for score 2. This subject had significant capsular fibrosis at necropsy, which may reduce laxity of the joint (39). The femoral head coverage measure was designed to assess risk of future degeneration onset secondary to DDH (40). A 5% reduction increased the odds of a lesion by a factor of 2.46 for 16-week coverage and 4.82 for 32-week coverage ($\chi^2 = 11.39$, $p < 0.001$ and $\chi^2 = 13.50$, $p < 0.001$, respectively).

Subluxation was measured as the percentage of the femoral head covered by the dorsal rim of the acetabulum. Greater subluxation corresponded to reduced femoral head coverage. At 16 weeks, the average femoral head coverage was 64.5% (SD 9.2) with a minimum of 45.4% and a maximum of 80.0%. At 32 weeks, the average femoral head coverage was 55.7% (SD 12.1) with a minimum of 28.0% and a maximum of 75.0% (Figure 2.4).

BMD Statistical Distribution

The statistical distribution of the calibrated SCO voxel values was evaluated at 7 ages with the first at 29.8 days (SD 2.04) and the last at 223.9 days (SD 6.11). The

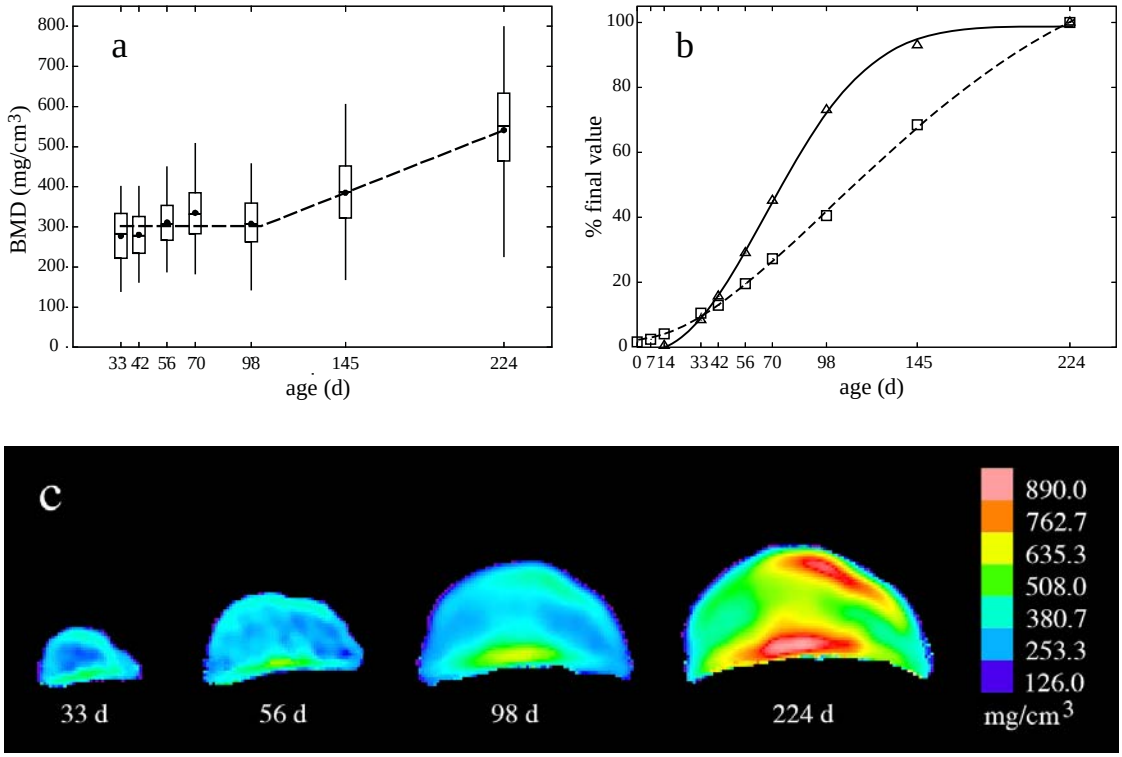

Figure 2.5 Example of BMD statistical distribution (a) and SCO volume and body weight growth curves (b). Maximum growth rates occurred at 66.5 days (SE 1.8) for volume and 92.1 days (SE 3.8) for body weight. Calibrated 2D images (c) from the location indicated in Figure 2.3 are shown for selected ages. Note the high BMD regions near the articular and capital femoral growth plate surfaces, and the developing column of moderate density bone connecting these regions at 98 and 224 days.

distribution for each SCO had a single central peak and was approximately symmetric, with the mean BMD within 6.4% of the median at all ages. After 140 days, the median value was consistently greater than the mean value, indicating a skew toward the lower portion of the density range (Figure 2.5a). At 29.8 days, the mean SCO BMD was 293.0 mg/cm^3 (SE 5.6). The mean BMD was not associated with body weight at 29.8 days ($F(1, 3.5) = 1.13$, $p = 0.355$). Females had a greater mean BMD than males (by 13.9 mg/cm^3), but the difference was not significant ($F(1, 10.6) = 2.21$, $p = 0.167$).

At 223.9 days, the mean BMD was 559.7 mg/cm^3 (SE 12.5), an average of 1.92 times (SE 0.05) the mean BMD at 29.8 days. The total variance was 2.43 times that at 29.8 days. The increase in variance was primarily due to accrual of high density bone near the articular and growth plate and surfaces (Figure 2.5c). The 32-week mean BMD was not associated with the 32-week body weight ($F(1, 11.1) = 0.05$, $p = 0.823$) or with gender ($F(1, 9.3) = 0.38$, $p = 0.554$). Reduced femoral head coverage at 32 weeks corresponded to a lower mean BMD (by −4.7 mg/cm^3 per 10% coverage reduction) ($t(16.5) = 1.40$, $p = 0.090$, 1-tail); the strength of the association was suggestive of significance. A 1-tailed *t*-test was performed because the alternative hypothesis was one-directional and stated that subluxation would be associated with a decrease in SCO mean BMD. The probability of a cartilage lesion increased as femoral head coverage decreased ($\chi^2 = 13.50$, $p < 0.001$), and as final body weight increased ($\chi^2 = 6.80$, $p = 0.009$). The probability of a lesion was not associated with mean BMD at 32 weeks ($\chi^2 = 0.17$, $p = 0.678$).

SCO Mean BMD Temporal Trajectory

The 3-parameter spline model provided a good fit to the individual SCO mean BMD temporal trajectories, accounting for 95.7% (SD 0.029) of the total variance (Figure 2.5a). The grand mean of the pre-knot slope for the 4-parameter model, S_1, was -0.28 mg/cm^3/d (SE 0.27); this was not significantly different from zero ($t(2.42) = -1.07$, $p = 0.381$). For the 3-parameter model, the constant pre-knot BMD value, β_0, was 301.1 mg/cm^3 (SE 10.6). Lower pre-knot BMD was associated with decreased 16- and 32-week femoral head coverage ($F(1, 21.9) = 13.63$, $p = 0.001$ and $F(1, 15.1) = 10.92$, $p = 0.005$, respectively). The probability of a lesion at 32 weeks increased as pre-knot BMD decreased ($\chi^2 = 5.71$, $p = 0.017$). The knot location for the

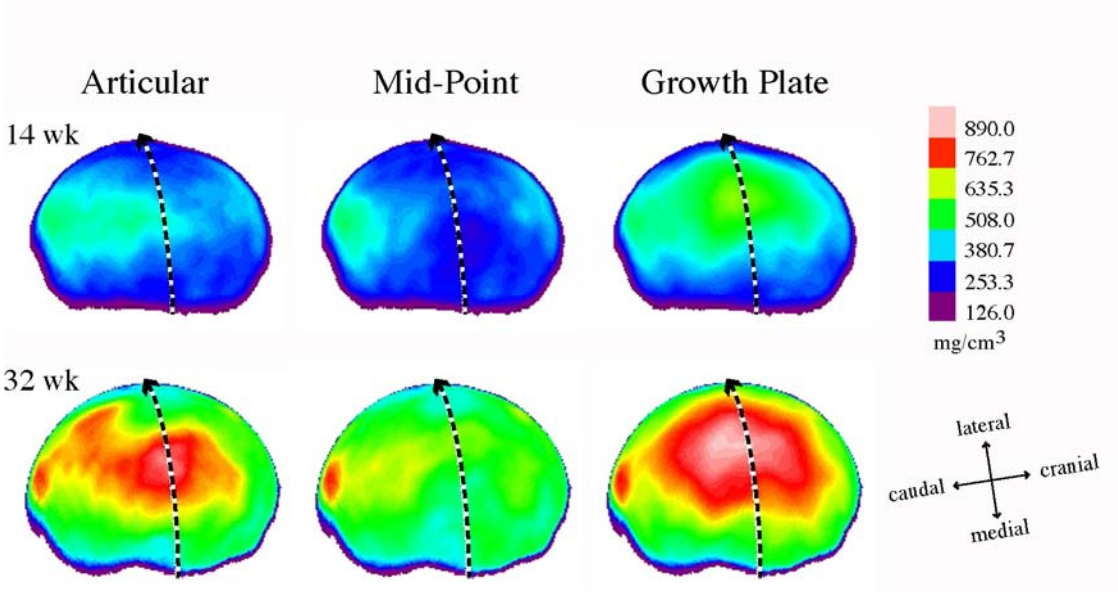

Figure 2.6 Example of BMD projections for 14-week (top row) and 32-week (bottom row) articular (column 1), mid-point (column 2), and growth plate (column 3) regions. Projections are shown for the same hip. The dashed lines represent the location of the 1D profile sample (Figure 2.3).

3-parameter model, κ, was 98.2 days (SE 12.6). The knot location corresponded to 69.5% (SE 11.7) of the 32-week volume of the SCO (Figure 2.5b, example trajectories). The post-knot slope, S_2, was 2.09 mg/cm^3/day (SE 0.12). The slope was not associated with gender ($F(1, 9.59) = 1.47$, $p = 0.254$), 32-week femoral head coverage ($F(1, 21.6) = 1.06$, $p = 0.315$), or the 32-week degeneration score ($\chi^2 = 0.30$, $p = 0.583$).

Spherical BMD Projections

The spatial variation of the BMD magnitude can be seen clearly in the spherical density projections (Figure 2.6). The articular and growth plate projections contain a central region of higher BMD. In contrast, the mid-point projection contains lower

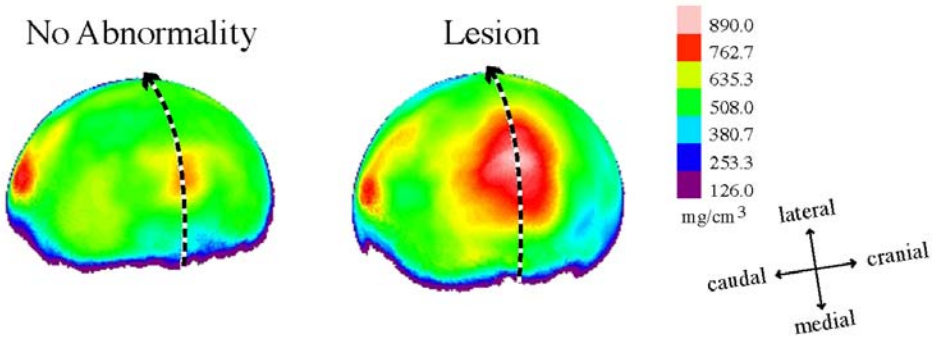

Figure 2.7 Spherical projections for the articular region of the no abnormality and lesion example hips in Figure 3.1. Note the larger area of high density bone represented in the lesion relative to the no abnormality projection. The dashed lines represent the location of the 1D profile sample (Figure 2.3).

BMD in the central region. The overall BMD magnitude increased from the 14- to the 32-week projections.

14 weeks: The high BMD region ($\geq 90^{th}$ percentile for all SCO voxels) corresponding to the articular surface accounted for 11.1% (SE 1.7) of the projection surface area. The high BMD region corresponding to the capital femoral growth plate accounted for 40.1% (SE 2.1) of the projection surface area. There was no significant relationship with femoral head coverage or the probability of cartilage lesion for either area.

32 weeks: The high BMD region corresponding to the articular surface accounted for 12.6% (SE 1.6) of the projection surface area. The proportion of high BMD area increased as femoral head coverage decreased (Figure 2.7). The association was not significant for 16-week coverage ($t(19.4) = -0.95$, $p = 0.176$, 1-tail), but was suggestive of significance for 32-week coverage ($t(22.1) = -1.50$, $p = 0.074$, 1-tail). A 1-tailed *t*-test was performed because the alternative hypothesis was one-directional and stated that subluxation would be associated with an increase in the size of the high

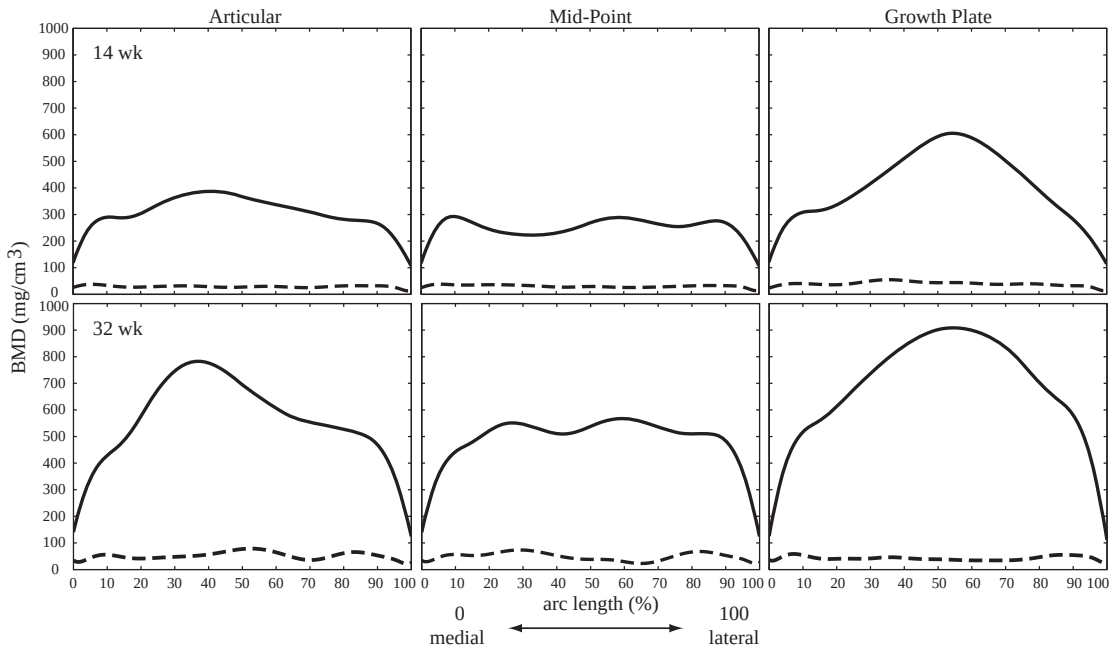

Figure 2.8 Point-by-point mean (solid) and standard deviation (dashed) curves for 1D BMD profile curves for 14 (top) and 32 (bottom) weeks (n = 28 hips).

density region associated with the articular surface. As the high BMD area increased, the probability of a cartilage lesion increased (χ^2 = 2.99, p = 0.084); the strength of the association was suggestive of significance. The high BMD region corresponding to the capital femoral growth plate accounted for 35.7% (SE 1.5) of the projected area. The proportion of high BMD area decreased with decreasing femoral head coverage at 16 weeks (F(1, 23.6) = 5.21, p = 0.032) and 32 weeks (F = (1, 17.5) = 3.74, p = 0.070). As the high BMD area decreased, the probability of a cartilage lesion increased (χ^2 = 5.18, p = 0.023).

Medial-Lateral BMD Profiles

The 1-dimensional medial-lateral BMD profiles for the articular and capital femoral growth plate regions exhibited a single main peak, while the midpoint profile was relatively constant over the central 90% of the normalized arc length (Figure 2.8).

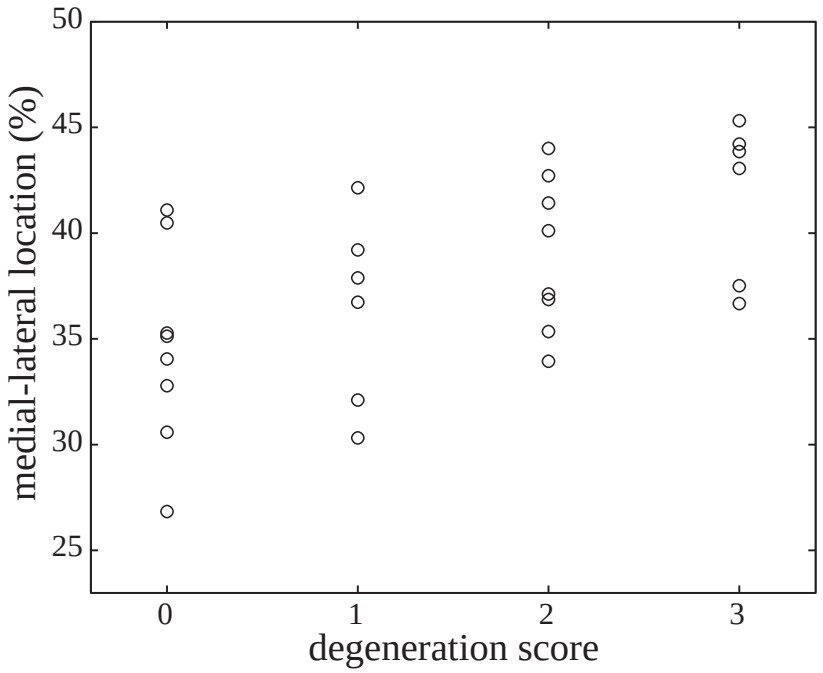

Figure 2.9 Peak MLL for articular BMD profiles (n = 28 hips). Score 0 indicates no abnormalities; score 3 indicates a lesion (see Table 2.1). A smaller MLL value indicates a more medial location.

Associations for femoral head coverage and degeneration score for the 14-week analysis are reported if they differ from those at 32 weeks.

Peak medial-lateral location: At 32 weeks, the mean MLL of the articular BMD profile peak was 37.8% (SE 1.4). Peak MLL was not associated with 16-week or 32-week femoral head coverage ($F(1, 18.7) = 0.00$, $p = 0.975$ and $F(1, 21.6) = 1.57$, $p = 0.223$, respectively), or with 32-week body weight ($F(1, 9.76) = 0.29$, $p = 0.605$). The probability of a cartilage lesion increased as MLL of the articular peak density increased ($\chi^2 = 8.61$, $p = 0.003$) (Figure 2.9). At 14 weeks, the mean MLL was 41.1% (SE 1.3). The probability of a cartilage lesion increased as the 14-week MLL increased ($\chi^2 = 2.68$, $p = 0.101$); the strength of the association was suggestive of significance.

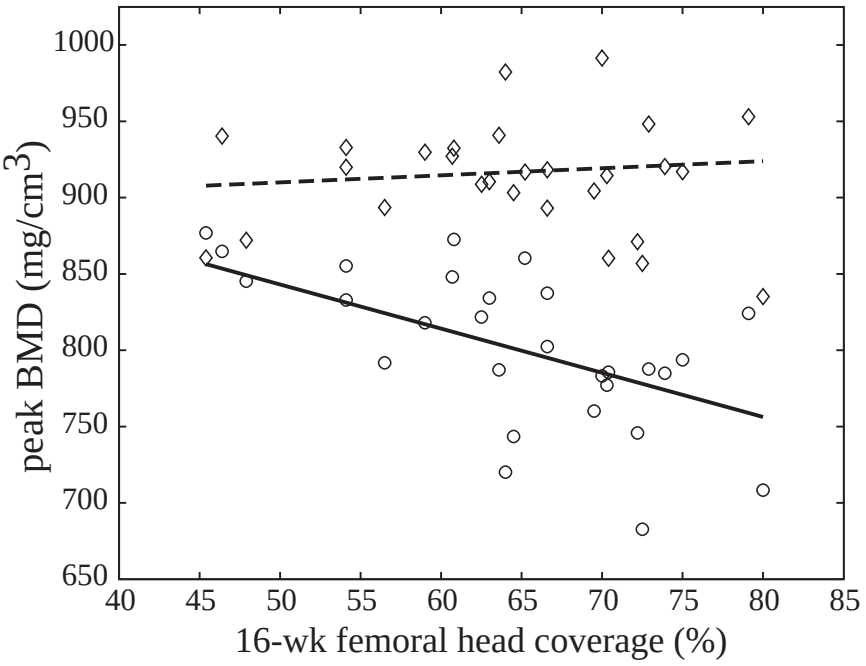

Figure 2.10 Peak BMD magnitude for articular (○, solid) and growth plate (◊, dashed) profiles (n = 28 hips). Lower femoral head coverage corresponds to increased subluxation.

At 32 weeks, the mean MLL of the capital femoral growth plate BMD profile peak was 55.1% (SE 1.0). Peak MLL was not associated with 16-week ($F(1, 23.3) = 1.21$, $p = 0.283$) or 32-week ($F(1, 14.7) = 1.16$, $p = 0.298$) femoral head coverage. Greater 32-week body weight was not associated with peak MLL ($F(1, 11.7) = 2.26$, $p = 0.160$). The probability of a cartilage lesion was not associated with the MLL of the growth plate peak BMD ($\chi^2 = 0.88$, $p = 0.348$). At 14 weeks, the mean MLL was 54.6% (SE 0.5).

Peak Magnitude: At 32 weeks, the mean magnitude of the articular BMD profile peak was 801.5 mg/cm^3 (SE 14.5). Greater peak magnitude was associated with lower 16-week ($t(25.9) = -3.05$, $p = 0.003$, 1-tail) (Figure 2.10) and 32-week ($t(19.5) = -3.03$, $p = 0.003$, 1-tail) femoral head coverage. A 1-tailed t-test was performed because the

alternative hypothesis was one-directional and stated that subluxation would be associated with a density increase at the site of load application. The probability of a cartilage lesion increased as articular peak magnitude increased ($\chi^2 = 5.12$, $p = 0.024$). At 14 weeks, the mean peak magnitude was 402.2 mg/cm^3 (SE 6.3). The 14 week mean magnitude was not associated with 16-week femoral head coverage ($t(22.3) = -1.30$, $p = 0.207$, 1-tail) or with the probability of a cartilage lesion ($\chi^2 = 0.27$, $p = 0.601$).

At 32 weeks, the mean magnitude of the capital femoral growth plate BMD profile peak was 916.4 mg/cm^3 (SE 15.4). Peak magnitude was not associated with 16-week ($F(1, 21.3) = 0.62$, $p = 0.439$) or 32-week ($F(1, 21.8) = 0.11$, $p = 0.738$) femoral head coverage. Greater peak magnitude was associated with greater 32-week body weight ($F(1, 12) = 9.89$, $p = 0.008$). The probability of a cartilage lesion was not associated with the peak magnitude ($\chi^2 = 0.05$, $p = 0.824$). At 14 weeks, the mean magnitude was 614.8 mg/cm^3 (SE 22.3).

At 32 weeks, the mean ratio of the articular peak magnitude to the growth plate peak magnitude was 0.88 (SE 0.01). A greater density ratio was associated with lower 16-week ($F(1, 25.8) = 9.97$, $p = 0.004$) and 32-week ($F(1, 17.8) = 6.19$, $p = 0.023$) femoral head coverage. The probability of a cartilage lesion increased as the ratio of articular to growth plate peak magnitudes increased ($\chi^2 = 4.82$, $p = 0.028$). At 14 weeks, the mean ratio was 0.66 (SE 0.03). The 14-week ratio was not associated with 16-week femoral head coverage ($F(1, 22) = 0.86$, $p = 0.363$) or with the probability of a cartilage lesion ($\chi^2 = 0.12$, $p = 0.731$).

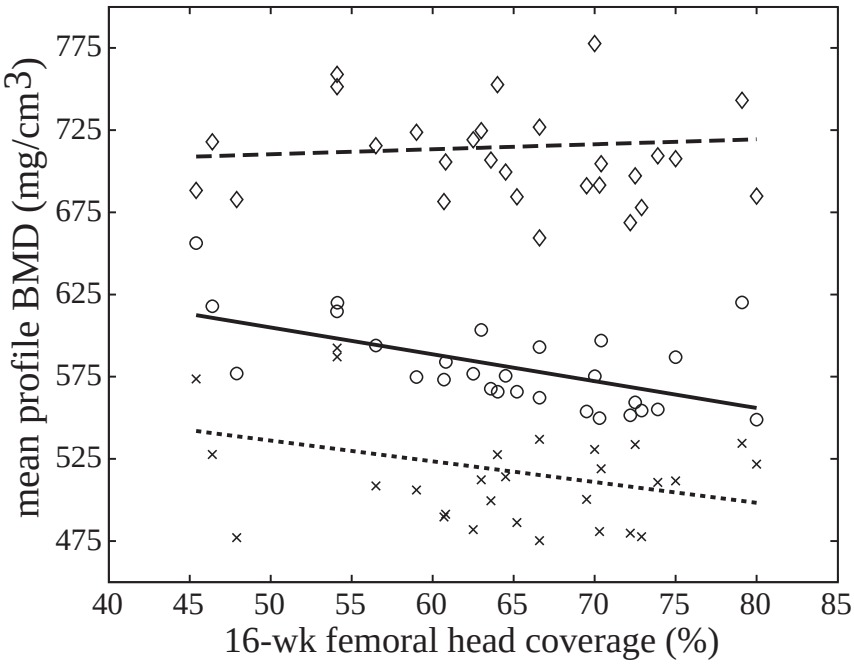

Figure 2.11 Mean BMD for articular (○, solid), growth plate (◊, dashed), and mid-point (×, dotted) profiles (n = 28 hips). Lower femoral head coverage corresponds to increased subluxation.

Profile Mean BMD: At 32 weeks, the mean BMD of the articular profile was 556.2 mg/cm^3 (SE 6.45). Mean profile BMD was greater for reduced 16-week (Figure 2.11) and 32-week ($F(1, 24) = 14.02$, $p = 0.001$ and $F(1, 20.1) = 6.28$, $p = 0.021$, respectively) femoral head coverage. Mean profile BMD was not associated with 32-week body weight ($F(1, 12) = 0.06$, $p = 0.814$). The probability of a cartilage lesion increased as mean profile BMD increased ($\chi^2 = 2.75$, $p = 0.097$); the strength of the association was suggestive of significance. At 14 weeks, the mean BMD was 304.9 mg/cm^3 (SE 6.6). The 14-week mean BMD was not associated with 16-week femoral head coverage ($F(1, 19.9) = 1.94$, $p = 0.179$).

At 32 weeks, the mean BMD of the capital femoral growth plate profile was 689.6 mg/cm^3 (SE 14.7). In contrast to the articular mean, the growth plate mean was not

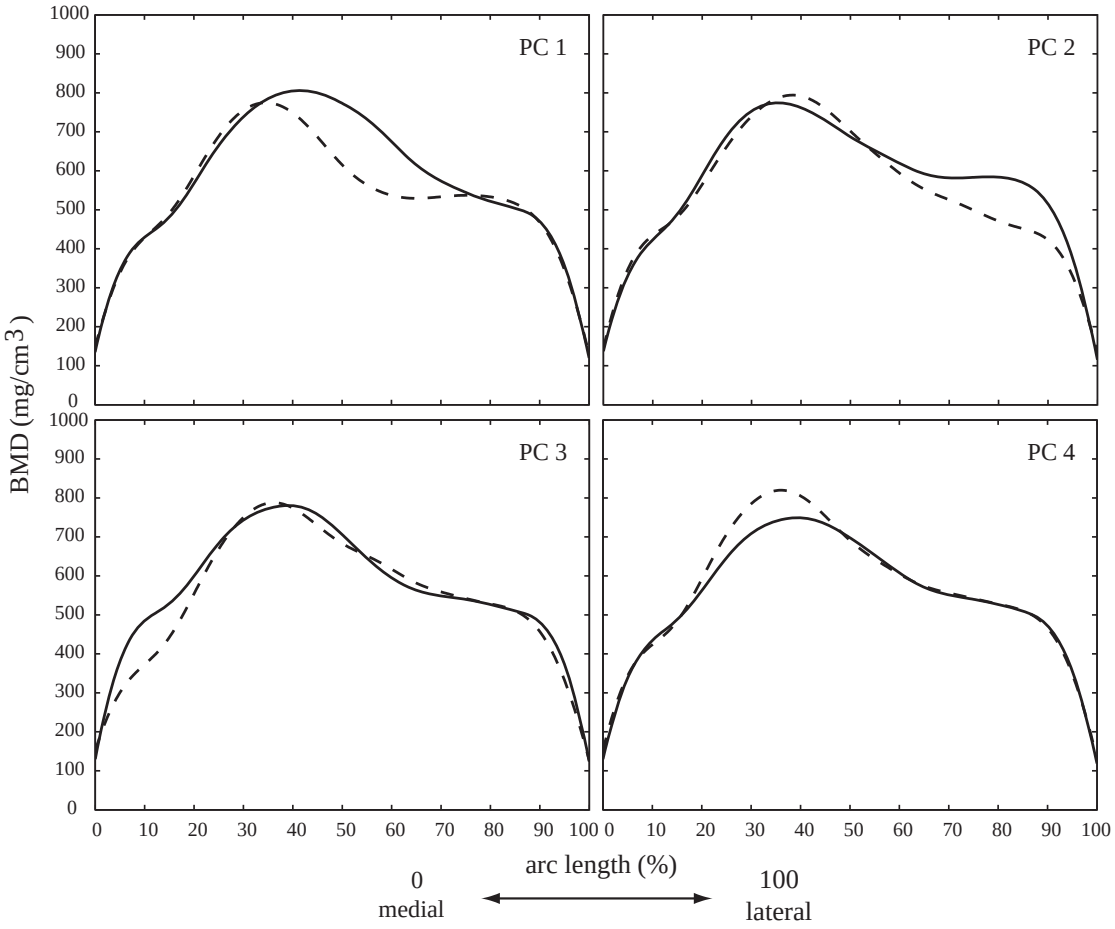

Figure 2.12 PC curves for articular region BMD profiles (n = 28 hips). PC 1 through 4 account for 38, 25, 14, and 14% of the total variance, respectively. The solid line represents $\bar{d} + 1s\xi(a)$ for that PC; the dashed line represents $\bar{d} - 1s\xi(a)$. s and ξ are the PC standard deviation and weight function, respectively.

associated with 16-week ($F(1, 22.9) = 0.36$, $p = 0.554$) or 32-week ($F(1, 13.9) = 0.01$, $p = 0.931$) femoral head coverage. Mean BMD was not associated with 32-week body weight ($F(1, 11.1) = 0.26$, $p = 0.620$). The probability of a cartilage lesion was not associated with the mean BMD of the growth plate profile ($\chi^2 = 0.09$, $p = 0.767$). At 14 weeks, the mean BMD was 409.0 mg/cm^3 (SE 15.4).

At 32 weeks, the mean BMD of the mid-point profile was 493.2 mg/cm^3 (SE 14.4). Mean profile BMD was greater for reduced 16-week ($F(1, 20.3) = 8.84$, $p = 0.007$),

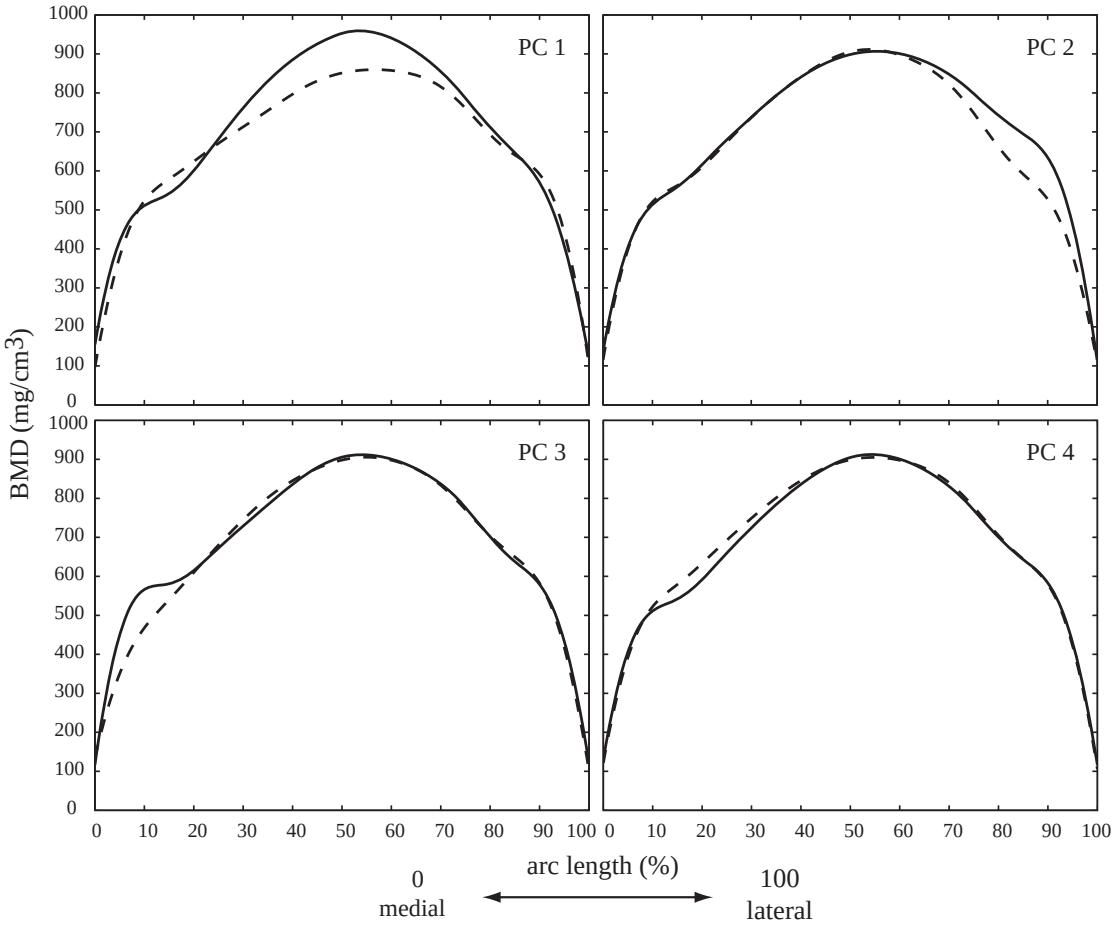

Figure 2.13 PC curves for growth plate region BMD profiles (n = 28 hips). PC 1 through 4 account for 29, 28, 17, and 17% of the total variance, respectively. The solid line represents $\bar{d} + 1s\xi(a)$ for that PC; the dashed line represents $\bar{d} - 1s\xi(a)$. s and ξ are the PC standard deviation and weight function, respectively.

but not 32-week ($F(1, 20.6) = 1.67$, $p = 0.211$), femoral head coverage. Mean BMD was not associated with 32-week body weight ($F(1, 10.9) = 1.30$, $p = 0.279$) or with the probability of a lesion ($\chi^2 = 0.04$, $p = 0.845$). At 14 weeks, the mean profile BMD was 253.4 mg/cm^3 (SE 10.0). The 14-week mean profile BMD was not associated with 16-week femoral head coverage ($F(1, 18) = 0.79$, $p = 0.387$).

32-week Principal Components: The 1st PC for the articular BMD profile corresponded to variation of the peak in width, MLL, and magnitude (Figure 2.12).

Higher PC 1 scores were associated with reduced 16-week and 32-week femoral head coverage ($F(1, 19.4) = 8.05$, $p = 0.010$ and $F(1, 20.2) = 9.32$, $p = 0.006$, respectively), and with greater probability of a cartilage lesion ($\chi^2 = 4.45$, $p = 0.035$). The 2nd PC corresponded to variation in height of the lateral shoulder of the profiles over the 65-90% range. PC 2 scores were not associated with 16- or 32-week femoral head coverage or with the probability of a cartilage lesion ($F(1, 22.6) = 0.04$, $p = 0.842$, $F(1, 22.4) = 0.27$, $p = 0.610$, and $\chi^2 = 0.85$, $p = 0.357$, respectively). The 3rd PC corresponded to variation in profile height over the 5-20% range. Higher PC 3 scores were also associated with reduced 16-week and 32-week femoral head coverage ($F(1, 23.6) = 7.77$, $p = 0.010$ and $F(1, 24) = 3.51$, $p = 0.073$, respectively). PC 3 scores were not associated with the probability of a cartilage lesion ($\chi^2 = 1.56$, $p = 0.212$). The 4th PC also corresponded to peak magnitude. Lower PC 4 scores were associated with reduced 16-week and 32-week femoral head coverage ($F(1, 23.2) = 10.31$, $p = 0.004$ and $F(1, 25.8) = 8.22$, $p = 0.008$, respectively). PC 4 scores were not associated with the probability of a cartilage lesion ($\chi^2 = 2.19$, $p = 0.139$).

The 1st PC for the capital femoral growth plate BMD profile corresponded to variation in peak magnitude (Figure 2.13). Lower PC 1 scores were associated with reduced femoral head coverage at 16 weeks ($F(1, 22.9) = 3.73$, $p = 0.066$); the strength of the association was suggestive of significance. Associations with 32-week femoral head coverage and the probability of a cartilage lesion were not significant ($F(1, 17.3) = 0.00$, $p = 0.993$ and $\chi^2 = 0.05$, $p = 0.817$, respectively). The 2nd PC corresponded to variation in height of the lateral shoulder of the profiles over the 70-95% range. PC 2 scores were not associated with 16- or 32-week femoral head coverage or with the probability of a cartilage lesion ($F(1, 24.9) = 0.06$, $p = 0.805$, $F(1, 18.4) = 0.01$, $p = 0.925$, and $\chi^2 = 0.18$, $p = 0.668$, respectively). The 3rd PC corresponded to variation

in profile height over the 5 to 17% range. Higher PC 3 scores corresponded to reduced 16-week femoral head coverage ($F(1, 22.1) = 3.17$, $p = 0.089$); the strength of the association was suggestive of significance. Associations with 32-week femoral head coverage and the probability of a cartilage lesion were not significant ($F(1, 14.4) = 1.95$, $p = 0.184$ and $\chi^2 = 2.50$, $p = 0.114$, respectively). The 4th PC corresponded to variation in profile height over the 10-40% range. PC 4 scores were not associated with 16- or 32-week femoral head coverage or with the probability of a cartilage lesion ($F(1, 21.5) = 0.33$, $p = 0.573$, $F(1, 13.0) = 0.27$, $p = 0.614$, and $\chi^2 = 0.39$, $p = 0.534$, respectively).

Discussion

DDH is a major cause of disability due to early onset OA; however, little is known about femoral head BMD development in the normal or subluxated hip. The objectives of this study were to use statistical and spatial analyses to evaluate the patterns of femoral head BMD that emerge during development, and to test for alterations of these patterns associated with the focal, eccentric loading characteristic of subluxation.

The serial data summarizing the statistical distribution of the calibrated QCT image voxels demonstrated the overall progression of BMD deposition during development. The mean and standard deviation of the BMD distribution were relatively constant until approximately 14 weeks, followed by a steep increase. After 14 weeks, the number of high density voxels increased while the lower portion of the distribution was nearly constant. The initial phase of volumetric growth acceleration corresponded to a relatively static BMD distribution, while the increase in high BMD values was seen after growth had begun to decelerate. The body weight growth curve exhibited a

more gradual increase than the SCO volumetric growth curve during the period from week 4 to 32. Subluxation was associated with lower mean BMD prior to 14 weeks. BMD for subluxated hips was lower than that for normal hips at 32 weeks; however, the difference was no longer significant. While alteration in hip articulation due to subluxation increases contact stress locally (41-43), the remainder of the femoral head experiences a reduced load. The average effect of the reduced loading was a reduced mean BMD during the early growth phase.

The maximum BMD spherical projection technique for SCO subsurface regions enabled evaluation of the local effects of joint contact alteration on the articular surface and capital femoral growth plate regions. The proportion of the projection area that was defined as high density was similar at 14 and 32 weeks. At 14 weeks, the proportions were not associated with subluxation. At 32 weeks, the proportion for the articular region high BMD area had increased for subluxated hips. The greater proportion was also associated with a greater probability of a cartilage lesion. In contrast, at 32 weeks, a decrease in the proportion of high BMD area for the capital femoral growth plate was associated with subluxation. The effect of focal, eccentric loading due to subluxation had a differential effect on the proportion of high BMD area for the articular and capital femoral growth region projections.

The 1-dimensional profiles of the BMD projections enabled measurement of the relative medial-lateral location (MLL) of the high BMD regions in a plane approximately perpendicular to the path of articulation. Higher peak MLL for the articular profile was associated with greater lesion probability; there was no difference for the growth plate. The peak and mean BMD for the articular profile increased with subluxation; there was no association for the growth plate. The effect of the focal,

eccentric loading due to subluxation was not yet apparent at 14 weeks. At 32 weeks, the profile peak MLL and the peak and mean BMD revealed a differential effect of subluxation on the articular and growth plate high density regions.

PCA of the spline-fitted, 1-dimensional BMD samples at 32 weeks provided a method to explore the dominant modes of variation in these profiles. Differences in articular profile peak MLL and magnitude were also demonstrated in this analysis. Additional differences associated with subluxation were a greater width of the density peak seen in PC 1 and a more rapid increase in density medially seen in PC 3. There was also significant variation in the density decrease in the lateral 40% of the arc length; but, this variation was not related to subluxation. For the capital growth plate, evaluation of the profile peak MLL and magnitude alone revealed no differences associated with hip subluxation. With PCA, lower PC 1 scores and higher PC 3 score associations with subluxation were detected. The PCA results demonstrated that the high BMD pattern for the growth plate was also affected by the focal, eccentric loading of subluxation; however, the effects were more subtle than those measured for the articular region.

A limitation of this study was the small sample size. *p*-values for several statistical tests approached, but did not reach, the conventional 0.05 level of significance. Most effects were strong enough to reach significance, so this was not a major limitation. The results of this research should be used to identify variables for further study. In the context of a preliminary study, the conventional alpha value for rejecting the null hypothesis should be increased to reduce the probability of accepting the null hypothesis when it is false.

Body weight was not significantly associated with most of the BMD features measured, as a consequence of the study design. Physical condition was very similar for all subjects because they were selected from the same breeding colony and given the same nutrition and exercise area. Variation in body mass index can be expected to be much higher in a naturally occurring population. Our focus was the effect of altered load application due to subluxation, not altered load magnitude due to variation in body mass index.

The 1-dimensional samples of the BMD projections were sufficient to demonstrate differences in peak location and magnitude of the high density regions due to altered loading; however, the femoral head cannot be well represented as a planar structure. Our results should motivate future efforts to analyze higher dimensional density distribution.

To our knowledge, this is the first study to quantify BMD patterns longitudinally and non-invasively during postnatal development for normal and dysplastic hips. Postnatal development of the femoral head SCO includes advancement of the ossification front and temporal changes in bone tissue, architectural, and mechanical properties. The femoral head SCO is composed of trabecular bone during development, with the subchondral shell appearing at maturity. The resolution of the QCT scans enabled measurement of volume averaged BMD that was dependent upon both the bone volume fraction and the extent of the tissue mineralization. As in mature bone (9), the mechanical properties of immature bone are strongly related to mineral density, with the relationship depending upon the stage of maturation (10,11,44). Experimental studies (11,44,45) have demonstrated that many changes take place with increasing age, including a decrease in trabecular connectivity density,

an increase in bone volume fraction, and an increase in tissue mineralization. Alignment of trabecular bone, measured as architectural anisotropy, increases with age and represents adaptation to the joint loading pattern (11,44,45). Alignment lags the increase in bone volume fraction (45) and may represent a phase of more specific adaptation to loading patterns following the initial period of rapid growth. In this study, a substantial increase in BMD did not occur until both body weight and SCO volumetric growth had begun to decelerate. This pattern suggests that during acceleration of growth, the primary response is the rapid formation of bone, and it is not until growth begins to decelerate that the majority of localized adaptation begins to occur.

Projection of subchondral bone density values – either maxima or from a fixed depth – have been used to evaluate bony adaptation to the prevailing load history for a variety of joints in adults (46,47). Finite element models of the elbow demonstrated a strong correspondence between the density distribution of the subchondral plate and loading patterns for a given morphology (48). In the developing joint, the subchondral plate does not yet exist; however, areas of high trabecular bone density were apparent just interior to the growth plate and the advancing articular growth front (Figure 2.5). In this study, two ages were evaluated during the period of growth deceleration and rapidly increasing BMD accrual. To our knowledge, this is the first time that subsurface BMD projection has been used to evaluate quantitatively the effect of subluxation on emerging mineralization patterns during hip development. The projections provided a platform for quantitative evaluation of *in vivo* hip function, and thus, risk of early OA onset.

Emergence of the high density structures described for mature femoral heads (12-14) was demonstrated in the articular and capital femoral growth plate regions. The beginning of the high density trabecular region connecting the high BMD regions was also visualized. The BMD patterns shown were not a transient feature of development, but, rather, an emerging pattern that persists in adulthood. These data can further inform mathematical modeling of joint development and diseases of maladaptation. Models that do not account for density patterns emerging during development generate a proximal femoral density pattern corresponding to the *in vivo* density distribution at a gross level (*e.g.* 49). Nevertheless, the utility of models with such general correspondence for better understanding the local changes that occur in mechanically-related developmental disease processes is questionable.

The increased contact stress due to focal, eccentric loading was sufficient to result in macroscopic lesions at 32 weeks (early skeletal maturity) in the hips with the greatest subluxation. Hips with moderate articular cartilage biochemical changes or macroscopic lesions were subjected to chronically elevated pressure for a sufficient period of time to induce the degenerative cascade of OA (2,3). The relationship between femoral head coverage and degeneration score (Figure 2.4) appears to have a dose-response nature with greater subluxation resulting in more severe degenerative changes by 32 weeks.

Increased subchondral bone density has long been associated with OA; however, whether these changes are primary to, secondary to, or concurrent with cartilage degeneration is still a matter of debate (50, review). In this study, the dose-response relationship between the articular cartilage degeneration score and femoral head coverage, in conjunction with the linear, inverse association between the peak BMD

magnitude and femoral head coverage, suggests that changes in cartilage and subchondral bone are concurrent responses to chronically elevated contact stress. The articular cartilage in hips with mild degenerative changes was abnormal; however, joint space narrowing due to tissue erosion may not have been apparent on plain radiographs for several years in this model. The increase in subchondral bone density may appear to precede cartilage changes in hips with a slower course of degeneration. Conclusions drawn regarding the temporal sequence of articular cartilage and subchondral bone degeneration are dependent on the method of observation used. Our results demonstrate that a hip with increased femoral head subchondral BMD is a hip at risk of degeneration.

In summary, differences in BMD patterns due to the focal, eccentric loading of subluxation were seen primarily in the articular region, with more subtle effects occurring at the growth plate. The effect of elevated contact stress has been shown to affect long term joint health (1); in this research, we demonstrate that joint development was affected as well. Changes in the mechanical stimuli due to hip subluxation resulted in measurable differences in the developing BMD pattern of the femoral head. These results support our contention that measures of BMD distribution can provide a basis for assessment of *in vivo* joint function during development, and for identifying hips at risk of early onset OA secondary to DDH.

Acknowledgments

The authors thank Dr. George Lust for his many years of research on canine DDH as both an important disease in veterinary medicine and as a naturally occurring model for human DDH. This work was made possible by the knowledge base that resulted from that research. The authors also thank Dr. Nathan Dykes for access to the CT

scanner, the Baker Institute for Animal Health, Cornell University, for access to the Labrador retriever breeding colony, and Sergei Fotin for coding the density projection algorithm. Support (W.S.V.B.-F.) was received from NSF and AAUW fellowships, and research was funded by a Cornell University College of Veterinary Medicine Consolidated Research Grant and New York State Advanced Technology Biotechnology Program Grant.

REFERENCES

1. Russell ME, Shivanna KH, Grosland NM, Pedersen DR 2006 Cartilage contact pressure elevations in dysplastic hips: a chronic overload model. J Orthop Surg 1:6

2. Hadley NA, Brown TD, Weinstein SL 1990 The effects of contact pressure elevations and aseptic necrosis on the long-term outcome of congenital hip dislocation. J Orthop Res 8:504-513

3. Maxian TA, Brown TD, Weinstein SL 1995 Chronic stress tolerance levels for human articular cartilage – 2 nonuniform contact models applied to long-term follow-up of CDH. J Biomech 28: 159-166

4. Weinstein SL 1987 Natural history of congenital hip dislocation (CDH) and hip dysplasia. Clin Orthop Relat Res 225:62-76

5. Shipman SA, Helfand M, Moyer VA, Yawn BP 2006 Screening for developmental dysplasia of the hip: a systematic literature review for the US Preventative Services Task Force. Pediatrics 117:e557-e576

6. Committee on Quality Improvement, Subcommittee on Developmental Dysplasia of the Hip 2000 Clinical practice guideline: early detection of developmental dysplasia of the hip. Pediatrics 105:896-905

7. McLeod KJ, Rubin CT, Otter MW, Qin YX 1998 Skeletal cell stresses and bone adaptation. Am J Med Sci 316:176-183

8. Jee WSS 2001 Integrated bone tissue physiology: anatomy and physiology. In: Cowin SC (ed) Bone Mechanics Handbook. CRC Press LLC, Boca Raton, pp 1.1-1.68

9. Lotz JC, Gerhart TN, Hayes WC 1990 Mechanical properties of trabecular bone from the proximal femur: a quantitative QCT study. J Comput Assist Tomogr 14:107-114

10. Koo MWM, Yang KH, Begeman P, Hemmami M, Koo WWK 2001 Prediction of bone strength in growing animals using noninvasive bone mass measurements. Calcif Tissue Int 68:230-234

11. Nafei, A, Danielsen CC, Linde F, Hvid I 2000 Properties of growing trabecular ovine bone, part I: Mechanical and physical properties. J Bone Joint Surg 82B:910-920

12. Stiehl JB, Jacobson D, Carrera G 2007 Morphological analysis of the proximal femur using quantitative computed tomography. Int orthop 31:287-292

13. Elke RPE, Cheal EJ, Simmons C, Poss R 1995 Three-dimensional anatomy of the cancellous structures within the proximal femur from computed tomography data. J Orthop Res 13:513-523

14. Edinger DT, Hayashi K, Hongyu Y, Markel MD, Manley PA 2000 Histomorphometric analysis of the proximal portion of the femur in healthy dogs. Am J Vet Res 61:268-274

15. Pressel T, Bouguecha A, Vogt U, Meyer-Lindenberg A, Behrens B-A, Nolte I, Windhagen H 2005 Mechanical properties of femoral trabecular bone in dogs. Biomed Eng Online 4:17

16. Riser WH 1975 The dog as a model for the study of hip dysplasia. Growth, form, and development of the normal and dysplastic hip joint. Vet Pathol 12:234-334

17. Lust G 1993 Other orthopedic diseases: hip dysplasia in dogs. In: Slater D (ed) Textbook of Small Animal Surgery. WB Saunders Company, Philadelphia, pp 1938-1944

18. Vanden Berg-Foels WS, Todhunter RJ, Schwager SJ, Reeves AP 2006 Effect of early postnatal body weight on femoral head ossification onset and hip osteoarthritis in a canine model of developmental dysplasia of the hip. Pediatr Res 60:549-554

19. Farese JP, Todhunter RJ, Lust G, Williams AJ, Dykes NL 1998 Dorsolateral subluxation of hip joints in dogs measured in a weight-bearing position with radiography and computed tomography. Vet Surg 27:393-405

20. Todhunter RJ, Bertram JE, Smith S, Farese JP, Williams AJ, Manocchia A, Erb HN, Dykes NL, Burton-Wurster NI, Lust G 2003 Effect of dorsal hip loading, sedation, and general anesthesia on the dorsolateral subluxation score in dogs. Vet Surg 32:196-205

21. Lust G, Todhunter RJ, Erb HN, Dykes NL, Williams AJ, Burton-Wurster NI, Farese JP 2001 Repeatability of dorsolateral subluxation scores in dogs and correlation with macroscopic appearance of hip osteoarthritis. Am J Vet Res 62:1711-1715

22. Gonzalez RC, Woods RE 2002 Digital image processing. Prentice Hall, Upper Saddle River, pp 123-124

23. Maes F, Colignon A, Vandermeulen D, Marchal G, Suetens P 1997 Multimodality image registration by maximization of mutual information. IEEE Trans Med Imaging 16:187-198

24. Cho ZH, Jones HP, Singh M, 1993 Foundations of medical imaging. Wiley & Sons, Inc, New York, pp 153-154

25. Reeves AP, Prokop RJ, Andrews SE, Kuhl FP 1988 Three-dimensional shape analysis using moments and Fourier descriptors. IEEE Trans Pattern Anal Mach Intell 10:937-943

26. Kostis WJ, Reeves AP, Yankelevitz DF, Henschke CI 2003 Three-dimensional segmentation and growth-rate estimation of small pulmonary nodules in helical CT images. IEEE Trans Med Imaging 22:1259-1274

27. Gille U, Salomon F-V 1995 Bone growth in ducks through mathematical models with special reference to the Janoschek growth curve. Growth Dev Aging 59:207-214

28. Singer JD, Willet JB 2003 Applied longitudinal data analysis: modeling change and event occurrence. Oxford University Press, Inc., New York, pp 102-103

29. Ruppert D, Wand MP, Carroll RJ 2003 Semiparametric regression. Cambridge. University Press, New York, pp 57-65

30. Reeves AP, Taylor RW 1989 Identification of three dimensional objects using range information. IEEE Trans Pattern Anal Mach Intell 11:403-410

31. Ramsay JO, Silverman BW 2006 Functional data analysis. Springer, New York, pp 1-49, 81-94. 147-164

32. Shumaker LL 1981 Spline functions: basic theory. John Wiley & Sons, New York, pp 118-138

33. de Boor C 2001 A practical guide to splines. Springer, New York, pp88-92

34. Johnson RA, Wichern DW 2007 Applied multivariate statistical analysis. Prentice Hall, Upper Saddle River, pp 430-507

35. Raudenbush SW, Bryk AS 2002 Hierarchical linear models: applications and data analysis methods. Sage, Thousand Oaks, pp 228-251

36. Searle SR, Casella G, McCulloch CE 1992 Variance components. John Wiley & Sons, Inc, New York, pp 1-18

37. Agresti A 2002 Categorical data analysis. JohnWiley & Sons, Inc, Hoboken, pp 274-282

38. Littell RC 2003 Analysis of unbalanced mixed model data: a case study comparison of ANOVA versus REML/GLS. J Agric Biol Environ Stat 7:472-490

39. Puerto DA, Smith GK, Gregor TP, LaFond E, Conzemius MG, Cabell LW, McKelvie PJ 1999 Relationships between results of the Ortolani method of hip joint palpation and distraction index, Norberg angle, and hip score in dogs. J Am Vet Med Assoc 214:497-501

40. Lust G, Williams AJ, Burton-Wurster N, Pijanowski GJ, Beck KA, Rubin G, Smith GK 1993 Joint laxity and its association with hip dysplasia in Labrador Retrievers. Am J Vet Res 54:1990-1999

41. Mavčič B, Pompe B, Antolič V, Daniel M, Iglič A, Kralj-Iglič V 2002 Mathematical estimation of stress distribution in normal and dysplastic human hips. J Orthop Res 20:1025-1030

42. Pompe B, Daniel M, Sochor M, Vengust R, Kralj-Iglič V, Iglič A 2003 Gradient of contact stress in normal and dysplastic human hips. Med Eng Phys 25:379-385

43. Burton-Wurster N, Farese JP, Todhunter RJ, Lust G 1999 Site-specific variation in femoral head cartilage composition in dogs at high and low risk for development of osteoarthritis: insights into cartilage degeneration. Osteoarthritis Cartilage 7:486-497

44. Nafei A, Kabel J, Odgaard A, Linde F, Hvid I 2000 Properties of growing trabecular ovine bone, part II: architectural and mechanical properties. J Bone Joint Surg 82B:921-927

45. Tanck E, Homminga J, Van Lenthe GH, Huiskes R 2001 Increase in bone volume fraction precedes architectural adaptation in growing bone. Bone 28:650-654

46. Müller-Gerbl M, Putz R, Kenn R 1992 Demonstration of subchondral bone density patterns by three-dimensional CT osteoabsorptiometry as a noninvasive method for in vivo assessment of individual long-term stresses in joints. J Bone Miner Res 7:S411-S418

47. Eckstein F, Müller-Gerbl M, Steinlechner M, Kierse R, Putz R 1995 Subchondral bone density in the human elbow assessed by computed tomography osteoabsorptiometry: a reflection of the loading history of the joint surfaces. J Orthop Res 13:268-278

48. Eckstein F, Jacobs CR, Merz BR 1997 Mechanobiological adaptation of subchondral bone as a function of joint incongruity and loading. Med Eng Phys 19:720-728

49. Bona MA, Martin LD, Fischer KJ 2006 A contact algorithm for density-based load estimation. J Biomech 39:636-644

50. Burr DB, Schaffler MB 1997 The involvement of subchondral mineralized tissues in osteoarthritis: quantitative microscopic evidence. Microsc Res Tech 37:343-357

CHAPTER 3

FEMORAL HEAD SHAPE IS ALTERED BY SUBLUXATION DURING DEVELOPMENT IN A CANINE MODEL OF HIP DYSPLASIA

Abstract

Developmental dysplasia of the hip (DDH) is characterized by joint malformation and early onset osteoarthritis (OA) at adulthood. Little is known about the effect of chronic, residual subluxation on the course of early postnatal hip development. The objective of this research was to quantify the evolving shape of the femoral head secondary center of ossification (SCO), and to test for associations between SCO shape, hip subluxation, and degeneration. Serial quantitative computed tomography and medial representation models were used to evaluate SCO shape noninvasively in a canine model of DDH. Thirty-four hips in 17 dogs were scanned at 7 ages from 4 weeks to early skeletal maturity at 32 weeks. Shape at 14 and 32 weeks was evaluated for this preliminary report. At 14 and 32 weeks, greater subluxation was associated with a thinner SCO in the perifoveal region, the characteristic site of articular cartilage lesion formation. Increased thinness of the SCO at this site was associated with a greater probability of degenerative changes. At 32 weeks, greater subluxation was also associated with a greater bend in the SCO lateral to the perifoveal region. The bend was not detected at 14 weeks. Analysis of the evolving SCO shape will improve our understanding of how chronic subluxation alters adult morphology of the femoral head and will improve our ability to detect hips at risk of early onset OA.

Introduction

Developmental dysplasia of the hip (DDH) is characterized by subluxation, a flattened femoral head, and a shallow acetabulum at adulthood (1). The abnormal shape results in greater contact pressure on portions of the articular surface and an increased risk of early onset osteoarthritis (OA) (2–5). In human neonates, DDH is characterized by joint laxity, ranging from mild subluxation to complete dislocation. The reported incidence of DDH in neonates ranges from 1.5 to 20 per 1000 births (6). As many as 1 in 100 hips exhibit evidence of instability at birth (7). A spontaneous resolution of the initial laxity was reported for 60% to 90% of hips evaluated with a follow-up examination (6). The levels of resolution reported varied with examination technique. The incidence of OA at adulthood for infants evaluated in screening studies is generally not available because symptoms of degeneration may not be evident for decades, even with early onset. For idiopathic hip OA, 20% to 50% of the cases have been attributed to subluxation or acetabular dysplasia (5), suggesting that the population incidence of DDH may be much higher than screening studies indicate.

Little is known about the effect of chronic overload due to subluxation on the course of early postnatal hip development. At birth, for humans and most other mammals, the majority of the femoral diaphysis has ossified while the proximal femur is still composed of cartilage. The cartilage is replaced by bone through the advancement of the primary ossification front and the initiation of secondary centers of ossification (SCO) (Figure 3.1). The femoral head SCO grows, through the process of endochondral ossification, to form the portion of the femoral head that articulates with the acetabulum. Bone can be regarded as a self-organizing system with properties that emerge in response to persistent environmental stimuli (8). Modeling and remodeling during growth produce skeletal structures that are mechanically adapted to the local

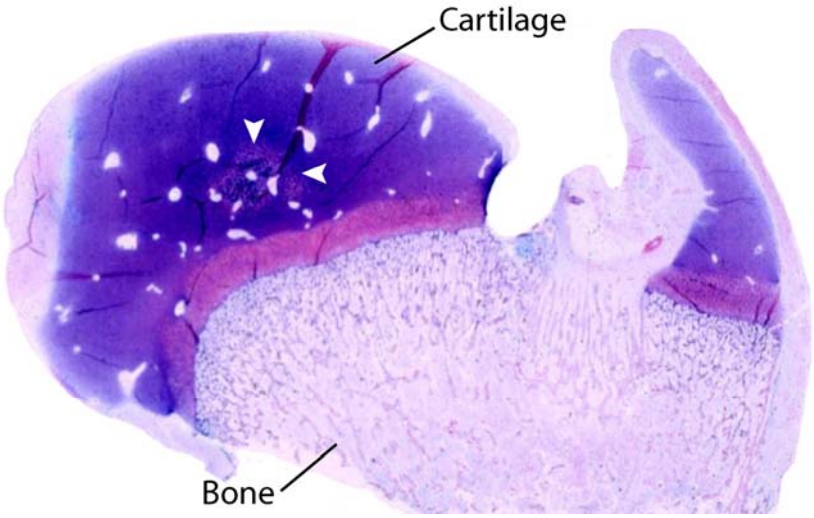

Figure 3.1 Proximal femur at 10 days of age. Mineralization of the SCO has begun (white arrowheads).

loading environment (9). Modeling results in site-specific alterations of architecture when mechanical loading changes, including altered patterns of bone mineral deposition and altered shape. Previous research evaluated the influence of subluxation on patterns of bone mineral deposition (10); the focus of this research was the influence of subluxation on the shape of the SCO during development.

Experimental animal studies have shown that the mechanical loading environment during development is an important factor in determining the adult morphology of the hip joint. A femur rudiment transplantation study in which loading was eliminated during development demonstrated that while the basic shape was still recognizable, mechanical loading was required to produce the characteristic refined structure of the proximal femur (11). Gross changes in femoral head and acetabulum morphology have been produced by joint dislocation or by splinting the hind limb with the knee in

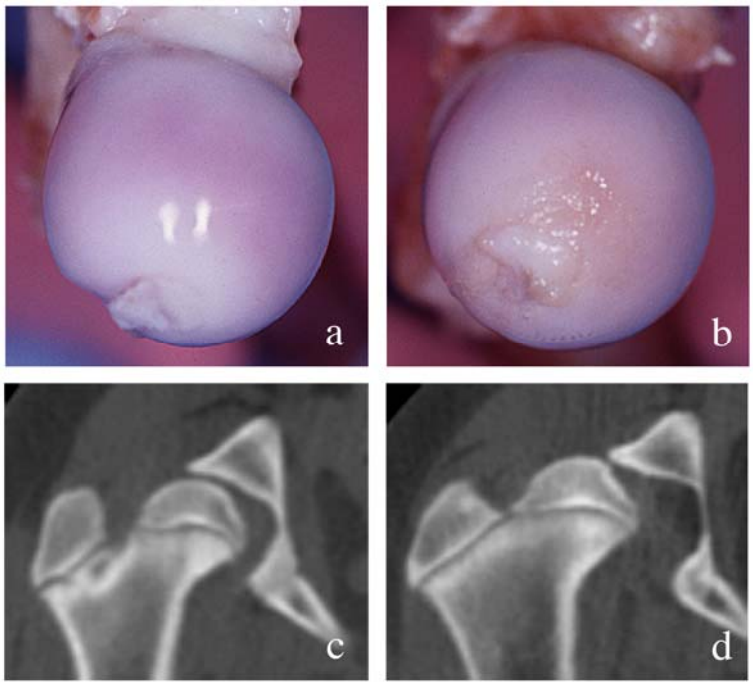

Figure 3.2 Articular surface of canine femoral heads at necropsy (a,b) with corresponding 32-week QCT images (c, d) for normal (b, d) and lesion (b, d) examples. Note cartilage roughness and focal, eccentric loading due to subluxation in lesion example.

full extension (12–15). What is unclear from the literature is the extent to which residual subluxation during development will affect the adult shape of the femoral head.

The objective of this study was to quantify the evolving shape of the femoral head SCO during development and to test the association of shape measures with hip subluxation and degeneration measures. The dog, a naturally occurring model of OA onset secondary to DDH, was used. The dog model has been previously described, and it shares many of the characteristic morphological and biochemical features of DDH in humans (5,16,17) (Figure 3.2). *In vivo* shape of the femoral head SCO was measured noninvasively using serial quantitative computed tomography (QCT) during

postnatal growth. Degeneration status of the hip was assessed at early skeletal maturity. We hypothesized that the shape of the SCO would be flattened (thinner) at the site of load application for hips with greater subluxation. We also expected that the overall shape of the SCO would be affected by subluxation; however, there was insufficient evidence in the literature on which to base a specific hypothesis. Analysis of the evolving SCO shape will improve our understanding of how chronic subluxation alters adult morphology of the femoral head and will improve our ability to detect hips at risk of early onset OA.

Methods

Experimental Design

The results reported here are the preliminary findings from a larger experimental study. The objective of the ongoing study is to characterize the shape of the femoral head SCO noninvasively during postnatal development, using serial QCT and medial-representation shape models. Scan ages for shape modeling were approximately 4, 6, 8, 10, 14, 24, and 32 weeks. The presence of hip joint degeneration was assessed at early skeletal maturity, approximately 32 weeks. A longitudinal design was chosen to quantify patterns of intra-individual shape change with age, and to evaluate the association of inter-individual SCO shape differences with subluxation and degeneration measures. The associations between SCO shape measures, joint subluxation, and degeneration status were examined. Here, we introduce model topology and fitting to the individual SCO images, and we report results for the 14- and 32-week analyses.

Animals

A sample of 17 Labrador Retrievers was obtained from a colony maintained by the Baker Institute for Animal Health, Cornell University, as has been previously described (18). Two to 4 dogs were randomly selected from the first 5 available litters. The phenotype of both sire and dam was either normal or dysplastic. The pattern of inheritance for hip morphology is complex; dysplastic offspring from phenotypically normal parents, and *vice versa*, are common. The sample included 9 females and 8 males. Enclosures provided area for exercise. This study was approved by the Cornell University Institutional Animal Care and Use Committee.

Radiography for Femoral Head Coverage

Femoral head coverage was measured at approximately 16 and 32 weeks using the dorso-lateral subluxation procedure (19,20). Femoral head coverage is strongly associated with development of OA secondary to DDH (21). Dogs were anesthetized and placed in sternal recumbancy on a positioning pad with stifles flexed and femora perpendicular to the table-top. The dorso-ventral radiographic projection was used to calculate the percentage of the femoral head area covered by the dorsal rim of the acetabulum.

Hip Joint Degeneration Score Assignment

At the conclusion of this study, at age approximately 32 weeks, a degeneration score was assigned based on necropsy evaluation and articular cartilage matrix component assays. Tissue collection, analysis, and score assignment have been described in detail previously (18). Joints were evaluated for gross changes characteristic of DDH associated degeneration, including effusion, hypertrophy of the femoral head ligament,

Table 3.1 Summary of assigned SCO degeneration scores

Score	Degeneration Status	Number of Hips
0	No abnormalities	9
1	Mild changes	7
2	Moderate changes	12
3	Macroscopic lesion present	6

capsule fibrosis, and macroscopic cartilage fibrillation. Biochemical assays of the superior perifoveal and surrounding cartilage were performed to measure the characteristic decrease in sulfated glycosaminoglycan and increase in water and fibronectin contents that occur in early OA. An ordinal degeneration score of 0 to 3 was assigned to each hip, with 0 representing no abnormalities and 3 representing a macroscopic lesion (Table 3.1).

QCT Image Acquisition and Processing

QCT image acquisition and processing have been described in detail previously (10). The temporal scan series had 1mm thick contiguous slices, with in-plane resolution ranging from 0.35×0.35 mm at 4 weeks to 0.78×0.78 mm at 32 weeks. Images were resampled to an isotropic voxel dimension of 0.25 mm using trilinear interpolation. Image super-sampling provided a smoother representation of the SCO surface and facilitated segmentation of the SCO from the proximal femoral neck.

SCOs were segmented from the surrounding tissue using a binary image mask. The mask was generated with a simple threshold at early ages or with iterative region

growing at advanced ossification. Manual intervention was occasionally required at advanced ossification to separate the SCO in regions of high growth plate curvature. A morphological opening was performed to remove any spurious boundary irregularities.

SCOs were placed in a standard orientation with respect to the image Cartesian coordinate axes using geometric moments (22,23). The SCO principal axes were aligned with the image coordinate axes via rigid body rotation: the major principal axis (largest eigenvalue) was aligned with the x-axis, the 2nd principal axis (2nd largest eigenvalue) was aligned with the y-axis, and the minor principal axis (smallest eigenvalue) was aligned with the z-axis. The SCO was not rotationally symmetric at any point during the evaluation period. Finally, the anatomical handedness of the SCO was standardized using a reflection operation. The left hip was chosen as the default and the right hip was reflected in the sagittal plane. The VisionX computer vision system (www.via.cornell.edu/visionx) was used as the basis for image processing operations.

Shape Modeling

Shape Representation: A medial representation method was selected for shape analysis because it provides a basis for the evaluation of local thickness and overall bending of an object (24). Landmark-based methods for shape analysis were not applicable because new bone is continually deposited on the surface as growth progresses and no bony prominences are present on the femoral head. The medial locus of an object can be formed by recording the center-point of all inscribed spheres that are bi-tangent to the surface (24). The positions of the sphere center-points $\mathbf{p}$ and corresponding radii r form the medial representation $\{\mathbf{p}, r\}$. The original boundary of

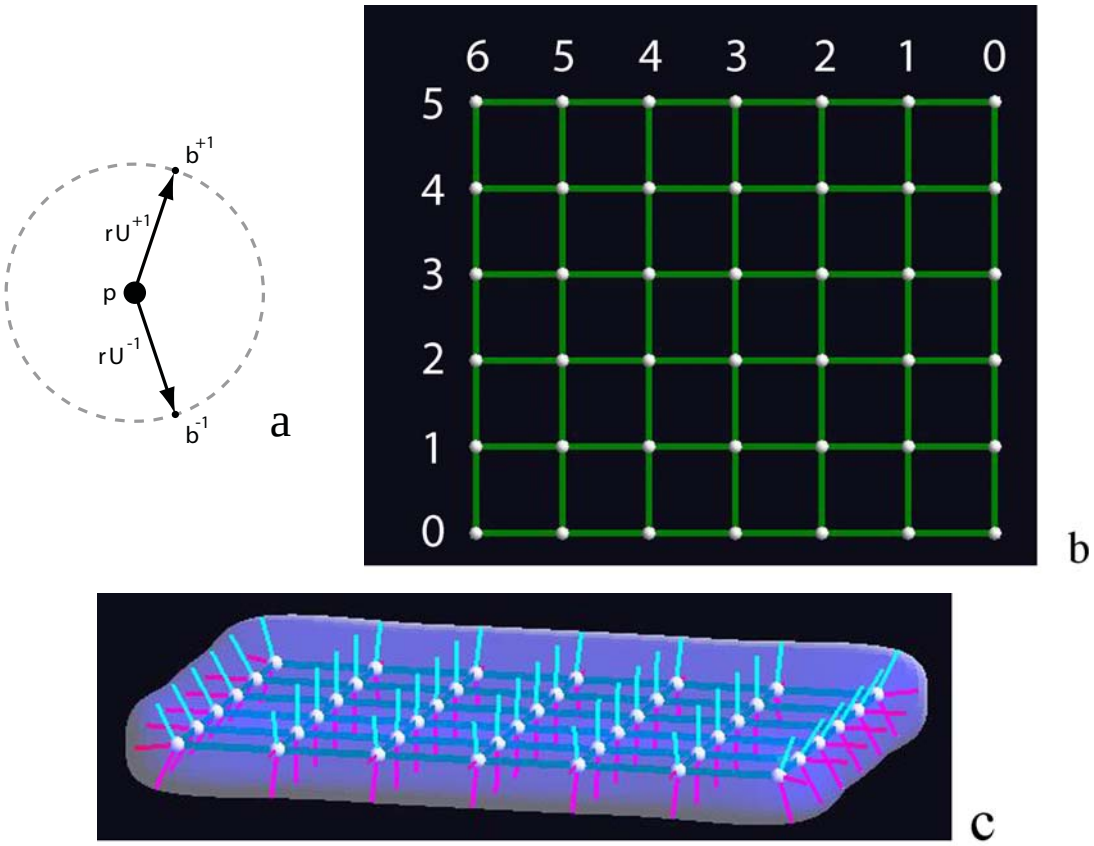

Figure 3.3 Interior medial atom with boundary points **b** defined by $\mathbf{b}^{\pm 1} = \mathbf{p} + r\mathbf{U}^{\pm 1}$ (see text) (a). Medial mesh of initial slab model was constructed from 6 rows by 7 columns of atoms (b). White spheres represent atom locations. Surface defined by medial mesh (c). Atom spokes defining surface boundary points are shown.

the object can be reconstructed by forming the union of all overlapping bi-tangent spheres. A boundary-derived medial representation, however, has several limitations, including topological changes of the medial structure in the presence of small-scale boundary variation or object deformation.

The shape model used in this study was based on the fixed and discretely sampled medial representation method introduced and advanced by Pizer and collaborators (24–26,29). The fixed medial topology was deformed to approximate the shape of each SCO. These shape models are typically referred to as m-reps. The fixed

topology provides a consistent basis for comparison across a population of similar objects and in the presence of object deformation. The common medial topology is also less sensitive to boundary noise than boundary-derived medial representations.

An m-rep consists of a mesh of linked medial primitives called atoms (Figure 3.3a,b). There are 2 types of atoms, end atoms that are located on the mesh periphery and interior atoms. In 3 dimensions, each interior atom is defined by a 4-tuple $m = \{\mathbf{p}, r, \mathbf{U}^{+1}, \mathbf{U}^{-1}\}$ with

$$\mathbf{p} \in \mathbb{R}^3, \quad r \in \mathbb{R}^+, \quad \mathbf{U}^{+1} \in S^2, \quad \mathbf{U}^{-1} \in S^2$$

where S^2 is the 2-dimensional unit sphere (disc) and $\mathbf{U}^{\pm 1}$ are unit vectors (referred to as spokes) that define the direction of the 2 surface tangent points with respect to the atom location. The 2 boundary points implied by a medial atom are given by $\mathbf{b}^{\pm 1} = \mathbf{p} + r\mathbf{U}^{\pm 1}$ (Figure 3.3a). Each end atom has an additional unit vector $\mathbf{U}^0$ and associated magnitude ηr that define a point on the crest of the implied boundary where $\mathbf{b}^0 = \mathbf{p} + \eta r \mathbf{U}^0$. A fully-connected model surface is formed from the m-rep by interpolation (Figure 3.3c).

M-rep Fitting: The m-rep template model was built manually on a single SCO at 32 weeks, the point at which the shape was most complex. A sufficient number of atoms were added to the template to ensure that at least one atom was associated with each surface feature. The m-rep configuration selected to represent all SCOs consisted of 42 atoms arranged in a 6 row by 7 column mesh (Figure 3.3b). The atom positions and radii of the slab model were edited manually to produce a template of the general SCO shape as the common starting point for the fitting procedure. Individual atoms were referenced by the mesh row and column positions.

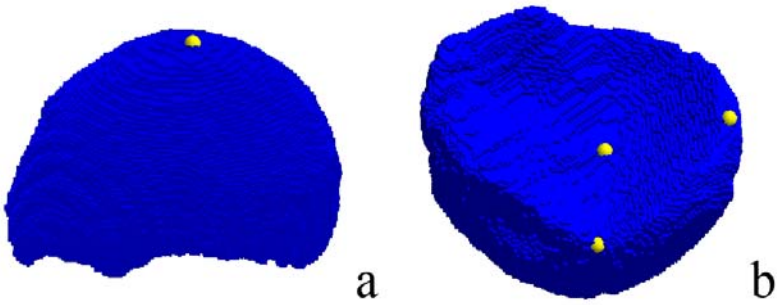

Figure 3.4 One landmark was placed on the dorsal surface of each binary image (a, yellow sphere); 3 landmarks were placed on the ventral surface (b).

An m-rep is deformed to fit the binary image of an object by working from the largest to the smallest scale (26,27). The smaller scale further refines the result of the fit at the larger scale. In the first, or initialization, stage, the template m-rep was geometrically aligned with and scaled to the binary SCO image using 4 user-defined landmarks (Figure 3.4). Three non-colinear landmarks were placed on the ventral surface and 1 landmark was placed on the dorsal surface. Each landmark was associated with an individual atom spoke. The landmarks represented the extremum of the ventral curvature, the most ventral location on the cranial border, and the dorsal pole. Because no bony landmarks exist, the placement of the landmarks was subjective. These landmarks were useful for establishing a consistent orientation and general positional correspondence across the sample of SCOs. At the second, or figure, stage, the medial sheet was warped as a whole. At the third, or atom, stage, individual atoms were adjusted to improve the m-rep fit. The objective function for the optimization included a mesh regularity measure, the sum of the squared distances between the image and implied boundary, and the sum of the squared distances between the image and the template landmark locations. In addition to inhibiting creases and folds in the medial mesh, the regularity penalty improves positional correspondence between m-reps within a population.

M-reps were designed for the statistical study of shape for a population of objects. Because magnification and rotation transformations are nonlinear, the mean and variance can not be properly evaluated using principal components analysis (26,28). Extension of principal component theory to symmetric spaces by (28) has provided a principal geodesic analysis methodology for the evaluation of shape mean and variance. The statistical description of the population can be used to improve the fit of a template m-rep for a population of objects by penalizing any shape that is an outlier in the shape space.

To fit the template m-rep to the longitudinal series of SCO images, the template was first fitted to the fourth (10 week) time-point for a randomly selected sample hip. The model at the fourth time point was then used as the basis for fitting the models at the third and fifth time-points. The SCO at 10 weeks represented an intermediate point in the progression from the immature to the mature SCO shape. Smaller deformations were required to fit models at adjacent points. A strong penalty was used to maintain mesh regularity during m-rep deformation. The m-reps fit for the example hip were then used as the templates for the corresponding time-points for all other hips. The first fitting iteration provided an initial estimate of the shape space that was refined in 2 additional fitting iterations. The fitted m-reps were used to generate the mean model and principal geodesic analysis of the shape space for the second fitting iteration. The fitting procedure was concluded after the third iteration because the boundary of the fitted m-reps closely approximated the boundary of the individual SCOs. The Binary Pablo software tool, available from the Medical Image Display and Analyis group at the University of North Carolina, Chapel Hill, was used for fitting m-reps to the binary SCO images (29).

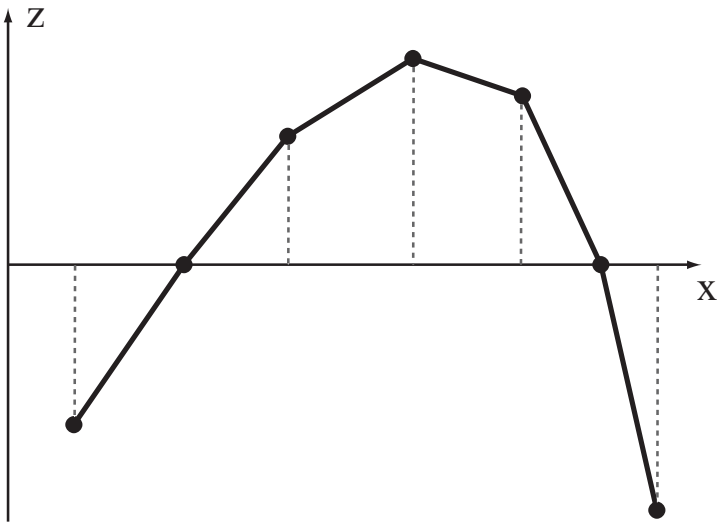

Figure 3.5 Z-axis height measurement of row 3 atoms (Figure 3.3b) for an example SCO. The circles represent individual atoms. The dashed lines mark locations of z-axis height measurement.

Size Normalization Each SCO was uniformly scaled to a unit volume, so measures of thickness and z-axis height were indicative of shape only, and not confounded with size.

M-rep Standard Orientation: All m-reps were placed in a standard orientation with respect to the x-y plane for z-axis height calculation. A translation and rigid body rotation were performed so that atom(3,1) and atom(5,5) locations were coincident with the x-axis. A rigid body rotation was performed so that atom(1,3) and atom(4,3) were at the same height above the x-y plane.

Shape Measures: The normalized radius (NR) of the maximum inscribed sphere was recorded for each atom location. The radius represented a size-normalized measure of the local thickness of the SCO. The normalized z-axis height (NZH) of the medial mesh was also recorded at each atom location (Figure 3.5). In a size-normalized

medial mesh with standard orientation, the z-axis height of the atoms indicated bending of the medial mesh. As bending of the medial mesh increased, the normalized z-axis height of the atoms increased.

Statistical Analyses

The association of the thickness and distance shape measures with the femoral head coverage and with the degeneration score was evaluated at individual atom locations. The *p*-values for the tests of significance were displayed in a grid with row and column positions corresponding to those of the atoms in the m-rep. Locations with significant associations were visualized by highlighting the corresponding atom positions in a representative m-rep.

As in the previous study utilizing this image set (10), these data also occurred in a natural hierarchical structure, with hips nested within dogs and dogs nested within litters. Observations are not independent, as hips within a dog are expected to be more similar than hips from different dogs, and dogs from the same litter are expected to be more similar than dogs from different litters. Hierarchical linear models (HLMs) explicitly address data dependency by using a sub-model for each level of the hierarchy; each submodel includes a level-specific error term (30).

A key feature of HLMs is that the total variance of the response variable is partitioned into portions contributed by individual levels. An unconditional 3-level random effects model contains a grand mean γ_{000} and 3 random error terms: u_{00k} for litter-level error, r_{0jk} for dog-within-litter error, and e_{ijk} for hip-within-dog error. The model for the dependent variable λ_{ijk} (NR, NZH) for hip *i* in dog *j* in litter *k* was

$$\lambda_{ijk} = \gamma_{000} + u_{00k} + r_{0jk} + e_{ijk}$$

where the variance was

$$\mathrm{var}(\lambda_{ijk}) = \mathrm{var}(u_{00k}) + \mathrm{var}(r_{0jk}) + \mathrm{var}(e_{ijk}) = \sigma^2_{litter} + \sigma^2_{dog} + \sigma^2_{hip}\,.$$

HLMs used included both the fixed effect of femoral head coverage and the random effects of litter, dog within litter, and hip within dog. See (31) for a review of effect classification in mixed models. The *p*-value of the slope coefficient for femoral head coverage in the conditional model was reported.

The 32-week hip degeneration score was an ordinal variable. A proportional odds model was used to estimate the effect of the independent variable on the log odds of a particular degeneration score (32):

$$\mathrm{logit}\left[P\left(score \le j\right)\right] = \alpha_j + \beta x, \quad j = 1,\ldots,J-1\,.$$

The model assumes that the effect of the independent variable *x*, NR or NZH, is the same (proportional) for all degeneration score categories. The *p*-value for the slope coefficient β was reported. The χ^2 test statistic for β had 1 degree of freedom.

The associations of the shape measures with femoral head coverage and degeneration score were evaluated for each atom individually. Observations within an m-rep model are spatially correlated because shape measures from adjacent atoms are generally more similar than shape measures from more distant atoms. This spatial correlation increases the likelihood of erroneously perceiving an association when one does not exist. This study was exploratory by design, due to the lack of previous research on the shape of the femoral head SCO, and the sample size was necessarily small, due to the high cost per dog of the project's longitudinal design. A relaxation of the false-positive error rate is appropriate in the exploratory context because the objective is to identify variables for more extensive analysis in future studies. The significance level for tests of association at the individual atoms was set at the conventional level of

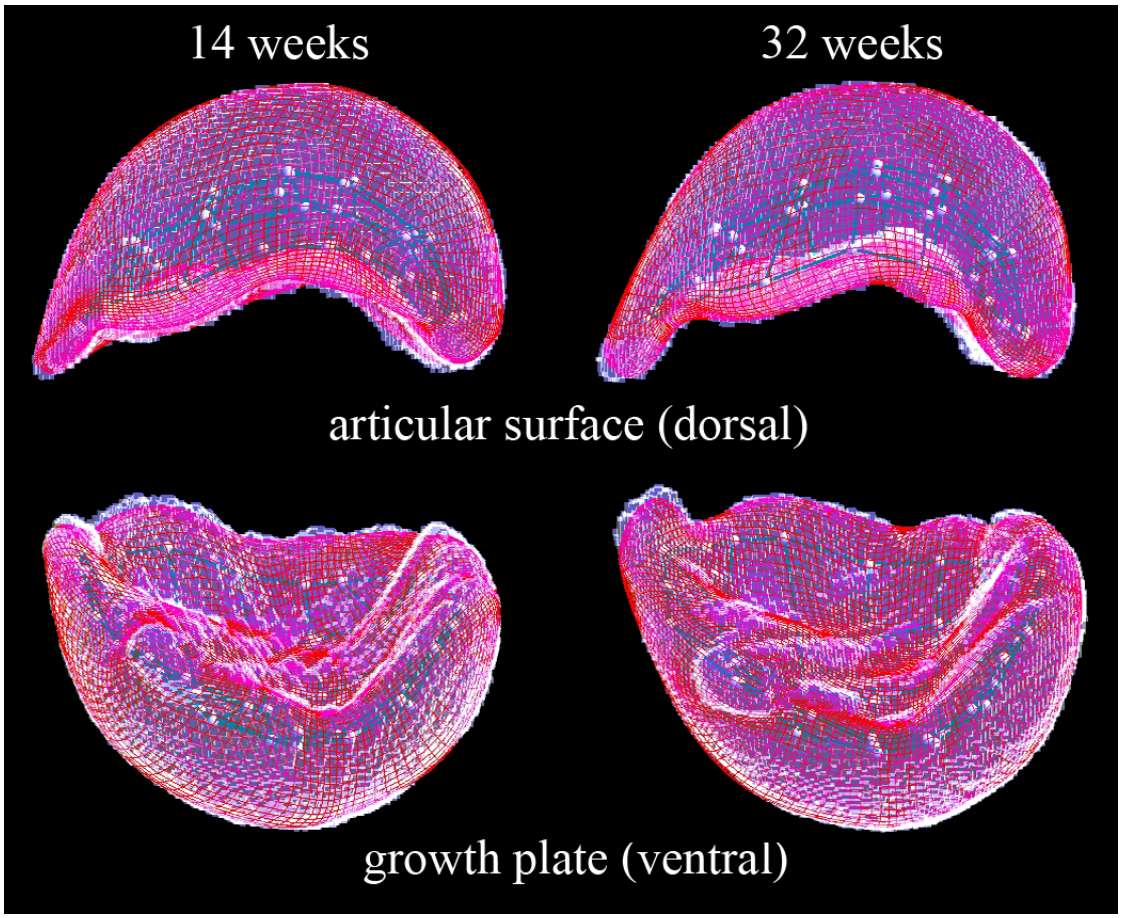

Figure 3.6 M-rep (red mesh) and binary image voxel (white) overlap for an example SCO at 14 and 32 weeks, with dorsal and ventral views.

0.05. Research on the multiple comparison problem due to spatial correlation is ongoing in the field of shape analysis (29).

An *a priori*, one-directional association of NR with subluxation and degeneration had been hypothesized for some atom locations. Because this was an exploratory study, atoms without an existing *a priori* hypothesis were also evaluated for association with subluxation or degeneration. One-tailed *p*-values were reported for atoms with a 1-directional alternative hypothesis; all other *p*-values were reported as 2-tailed. The

distinction between atoms with and without *a priori* hypotheses is indicated on the probability grids (Table 3.2, 3.3).

HLMs were implemented using the MIXED procedure in the SAS statistical software package (version 9.1, SAS Institute, Cary, NC). The restricted maximum likelihood procedure was used to estimate the variance partition. The Kenward-Roger approximation for unbalanced data (33) was used to estimate the degrees of freedom for *F* statistics. Estimated degrees of freedom are determined by the degree of data dependency and are often fractional. Proportional odds models were implemented using the LOGISTIC procedure in SAS.

Results

The 14- and 32-week m-reps were evaluated for this preliminary report. Deformation of the 42-atom m-rep topology (6 rows, 7 columns) resulted in a close approximation of the SCO boundary at 14- and 32-weeks (Figure 3.6). No folds were present and mesh regularity was maintained. The m-rep extended into the sharp crest at the junction of the articular (dorsal) and growth plate (ventral) surfaces. The m-rep was also able to represent accurately the undulating growth plate and the relatively smooth articular surfaces simultaneously.

A significance grid was constructed to evaluate the atom-by-atom association of the normalized radius (NR) with 32-week femoral head coverage (Table 3.2) and degeneration score (Table 3.3). Because all SCOs were scaled to a unit volume, the NR represented a measure of local thickness that was not confounded by size.

Table 3.2 Association of 14- and 32-week radii with 32-week femoral head coverage. Significant *p*-values correspond to atom locations highlighted in Figure 3.7. *p*-values within the bold box are 1-directional, all others are 2-directional.

32 weeks

	6	5	4	3	2	1	0
5	0.569	0.129	0.577	0.140	0.722	0.749	0.786
4	0.651	0.084	**0.028***	0.753	0.199	0.825	0.244
3	0.507	0.214	0.130	0.315	0.172	**0.028***	0.180
2	0.856	0.810	0.584	0.069	**0.003***	0.238	0.066
1	0.634	0.845	0.535	0.163	0.272	0.138	0.075
0	0.888	0.329	0.137	0.282	0.059	**0.019***	0.145

14 weeks

5	0.763	0.822	0.990	0.404	0.895	0.390	0.438
4	0.839	0.422	0.546	0.843	0.803	0.314	0.888
3	0.297	0.921	**0.015***	0.179	0.117	0.225	0.372
2	0.429	0.374	0.965	0.252	**0.015***	0.106	0.462
1	0.372	0.465	0.675	0.056	0.054	**0.049***	0.975
0	0.320	0.254	0.757	0.092	0.385	0.668	0.241

At 14 and 32 weeks, lower 32-week femoral head coverage was associated with a thinner SCO (smaller NR) at atom(2,2) ($t(20.2) = 2.33$, $p = 0.015$ and $t(19.5) = 3.09$, $p = 0.003$, respectively) (Figure 3.7). The strength of the association was stronger at 32 weeks. Association of NR with femoral head coverage was significant at 3 other atom locations at 32 weeks: lower femoral head coverage was associated with a thinner SCO at atom(3,1) and atom(4,4) and with a thicker SCO at atom(0,1) ($t(19.1) = 2.04$, $p = 0.028$, $F(1,31.7) = 5.34$, $p = 0.028$, and $F(1,19.1) = 6.60$, $p = 0.019$, respectively).

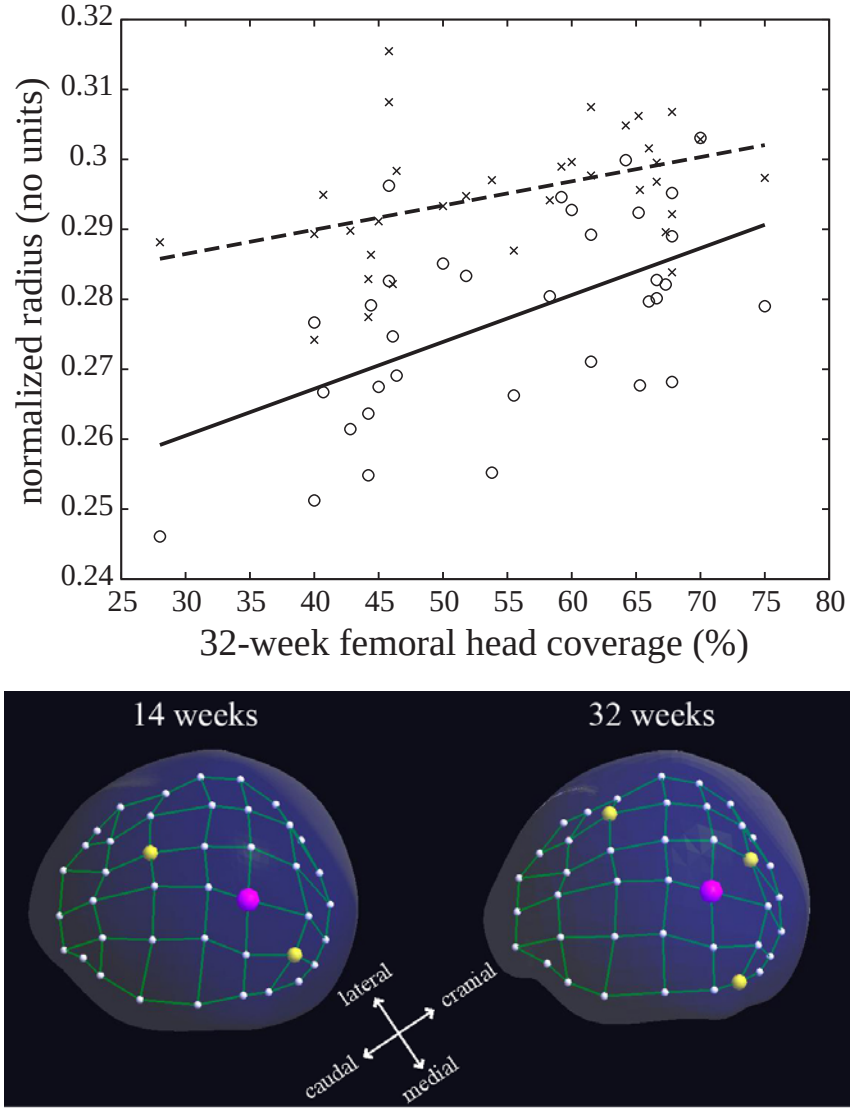

Figure 3.7 Size-normalized radius for 14 (×, ---) and 32 (○, —) weeks (n = 34 hips). Atoms with $p \leq 0.05$ are highlighted with larger colored spheres in the lower panel; the plotted radii are magenta. Lower femoral head coverage corresponds to greater subluxation.

At 14 weeks, the SCO was thinner at atom(1,1) and atom(3,4) ($t(16) = 1.75$, $p = 0.049$ and $F(1,30.8) = 6.69$, $p = 0.015$, respectively).

At 14 and 32 weeks, a smaller radius (thinner SCO) at atom(2,2) was associated with a higher probability of a lesion ($\chi^2 = 3.81$, $p = 0.051$ and $\chi^2 = 8.27$, $p = 0.004$,

Table 3.3 Association of 14- and 32-week size-normalized radii with degeneration score. Significant *p*-values correspond to atom locations highlighted in Figure 3.8. The bold box delineates the region in which a smaller radius (thinner) was expected to have a greater probability of degenerative changes.

32 weeks

	6	5	4	3	2	1	0
5	0.308	0.400	0.848	**0.031***	0.243	0.255	0.578
4	0.949	0.058	0.053	0.528	0.244	0.766	0.296
3	0.863	0.268	0.580	0.197	0.650	0.234	0.367
2	0.247	0.321	0.071	0.384	**0.004***	0.947	0.134
1	0.103	0.788	0.989	0.091	0.454	0.661	0.085
0	0.543	0.418	**0.020***	0.984	0.069	**0.012***	0.141

14 weeks

5	0.891	0.865	0.976	0.864	0.709	0.168	0.630
4	0.995	0.243	0.951	0.588	0.917	0.834	0.560
3	0.440	0.594	0.597	0.541	0.703	0.454	0.685
2	0.624	0.332	0.239	0.569	**0.051***	0.675	0.935
1	0.343	0.970	0.563	0.575	0.146	0.216	0.625
0	0.732	0.832	0.458	0.945	0.425	0.400	0.968

respectively) (Figure 3.8). The association was stronger at 32 weeks. There were no other atom locations with a significant association at 14 weeks. At 32 weeks, a thinner SCO at atom(5,3) and atom(0,4) was associated with a higher probability of a lesion ($\chi^2 = 4.68$, $p = 0.031$ and $\chi^2 = 5.41$, $p = 0.020$, respectively). A thinner SCO at atom(0,1) was associated with a lower probability of a lesion ($\chi^2 = 6.39$, $p = 0.012$).

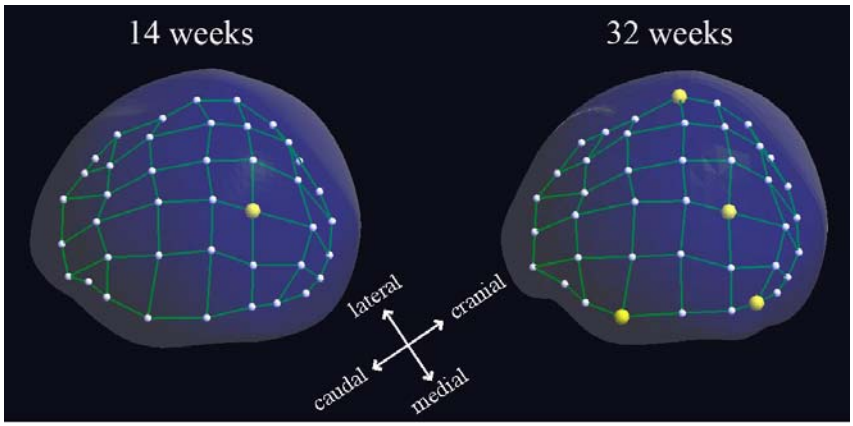

Figure 3.8 Atoms with a significant association between size-normalized radius and degeneration score are highlighted with larger yellow spheres.

A significance grid was also constructed to evaluate the atom-by-atom association of the normalized z-axis height (NZH) with 32-week femoral head coverage (Table 3.4) and degeneration score (Table 3.5). Because all SCOs were scaled to a unit volume and placed in a standard orientation, the NZH represented a measure of bending for the medial mesh.

Lower 32-week femoral head coverage was associated with a greater 32-week NZH (greater bending) ($F(1,31.1) = 8.34$, $p = 0.007$) (Figure 3.9). Lower femoral head coverage was also associated with greater bending at atom(2,4) and atom(3,3) ($F(1,24.7) = 6.83$, $p = 0.015$ and $F(1,17) = 6.65$, $p = 0.020$, respectively). NZH at atom(0,3) was negative (below the x-y plane), with lower femoral head coverage associated with a smaller NZH magnitude ($F(1,18.9) = 6.00$, $p = 0.024$). There were no significant associations between 32-week femoral head coverage and NZH at 14 weeks.

Table 3.4 Association of 14- and 32-week size-normalized z-axis height with 32-week femoral head coverage. Significant *p*-values correspond to atom locations highlighted in Figure 3.9. Atom(3,5) and atom(3,1) were aligned with the x-axis; z-axis height was zero. These atoms are denoted by x in the table.

32 weeks

	6	5	4	3	2	1	0
5	0.168	0.313	0.358	0.617	0.170	0.318	0.190
4	0.718	0.726	0.691	0.329	0.247	0.316	0.378
3	0.882	x	**0.007***	**0.020***	0.393	x	0.422
2	0.740	0.854	**0.015***	0.252	0.496	0.677	0.887
1	0.665	0.495	0.884	0.329	0.985	0.558	0.472
0	0.968	0.803	0.719	**0.024***	0.387	0.350	0.672

14 weeks

5	0.551	0.322	0.812	0.8477	0.803	0.115	0.274
4	0.530	0.867	0.768	0.102	0.814	0.077	0.419
3	0.935	x	0.605	0.235	0.573	x	0.769
2	0.075	0.891	0.923	0.282	0.239	0.347	0.768
1	0.204	0.625	0.976	0.102	0.742	0.077	0.286
0	0.503	0.296	0.232	0.881	0.620	0.791	0.358

At 32 weeks, 7 locations had a positive association between NZH and lesion probability. The strongest association was located at atom(3,3) ($\chi^2 = 7.00$, $p = 0.008$) (Figure 3.10). All χ^2 test statistics are listed by location in Table 3.6. There were no significant associations between 14-week NZH and lesion probability.

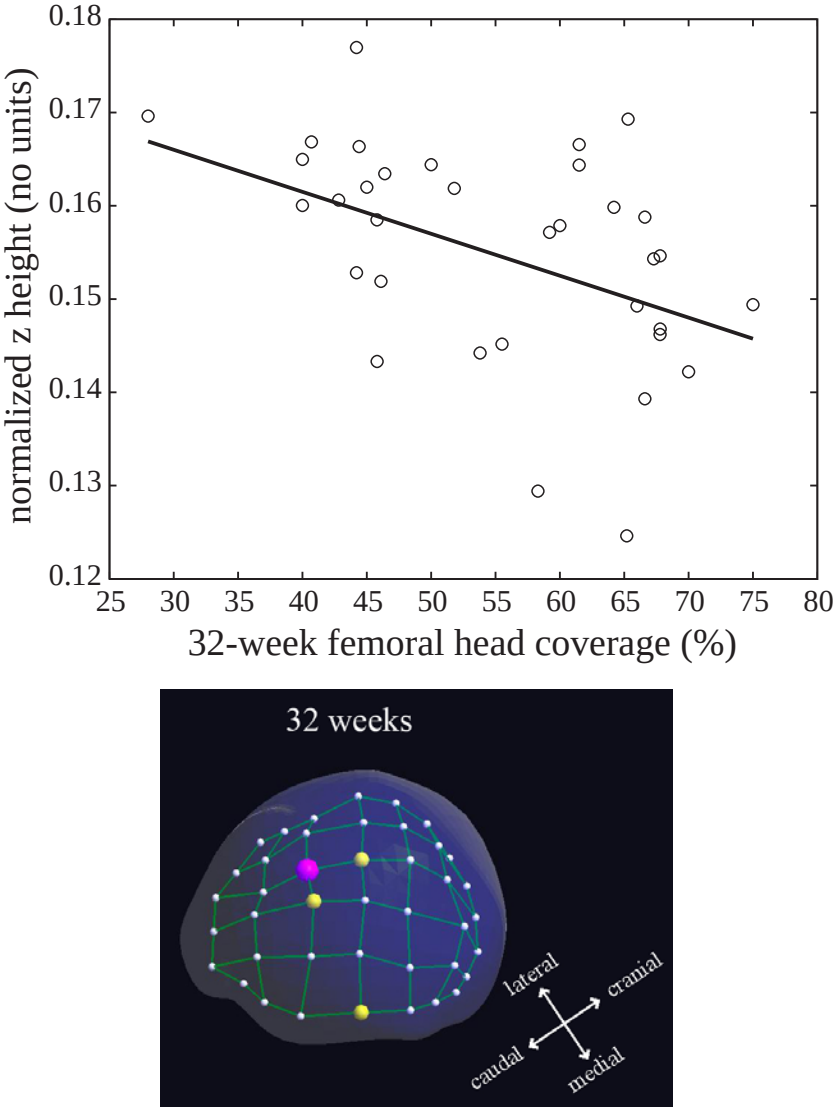

Figure 3.9 Size-normalized z-axis height for 32 weeks (n = 34 hips). Atoms with $p \leq 0.05$ are highlighted in the lower panel with larger colored spheres; the plotted radius is magenta. Lower femoral head coverage corresponds to greater subluxation.

Discussion

Little is known about the effect of chronic, mild subluxation during postnatal development on the shape of the femoral head at maturity. The objective of this preliminary report was to examine the association of SCO shape at 14 and 32 weeks with subluxation and degeneration.

Table 3.5 Association of 14- and 32-week size-normalized z-axis height with degeneration score. Significant *p*-values correspond to atom locations highlighted in Figure 3.10. Atom(3,5) and atom(3,1) were aligned with the x-axis; z-axis height was zero. These atoms are denoted by x in the table.

32 weeks

	6	5	4	3	2	1	0
5	0.473	0.439	0.732	0.905	**0.045***	**0.039***	0.135
4	0.774	0.991	0.758	0.435	**0.026***	0.105	0.070
3	0.766	x	**0.012***	**0.008***	0.378	x	0.355
2	0.684	0.607	**0.010***	0.454	0.481	0.791	0.522
1	0.261	0.794	0.932	0.435	0.468	0.938	0.291
0	0.550	0.486	0.422	**0.011***	0.992	0.109	0.215

14 weeks

5	0.891	0.518	0.747	0.918	0.671	0.849	0.820
4	0.999	0.860	0.989	0.511	0.933	0.406	0.847
3	0.815	x	0.417	0.253	0.859	x	0.353
2	0.984	0.719	0.847	0.771	0.944	0.306	0.852
1	0.956	0.734	0.891	0.511	0.228	0.064	0.201
0	0.943	0.899	0.715	0.561	0.156	0.757	0.358

A shape model based on a common medial representation (24–26,29) was fitted to each of the binary SCO images. The 42-atom medial mesh was a parsimonious model that could closely approximate the growth plate and articular surfaces simultaneously. Positional correspondence of the atom locations was established with user-defined landmarks and a mesh regularity penalty. The medial representation enabled the separate evaluation of SCO bending and local changes in thickness.

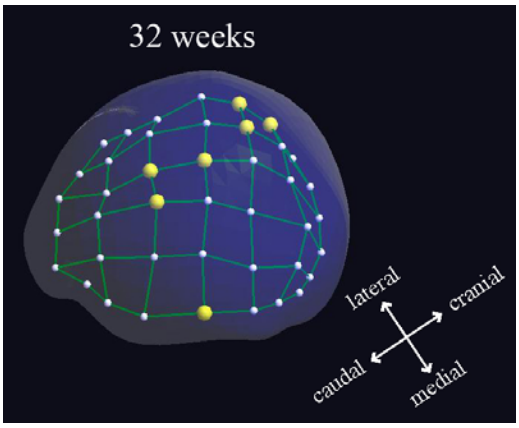

Figure 3.10 Atoms with a significant association between size-normalized z-axis height and degeneration score are highlighted with larger yellow spheres.

Lower femoral head coverage was associated with local thinning of the SCO at 14 and 32 weeks. The location of the significant association corresponded to the superior, perifoveal region that is characteristic for lesion formation (18,34). The probability of degenerative changes was higher for SCOs that were thinner in this location. The effect was more pronounced at 32 weeks (early maturity) than at 14 weeks. The relationship between femoral head coverage and the superior, perifoveal thickness (Figure 3.7) appears to be of a dose-response nature with greater subluxation resulting in a locally thinner SCO. A larger area of high density subchondral bone in the superior, perifoveal region has also been associated with lower femoral head coverage (10). Together these studies suggest that focal, eccentric loading inhibits the advancement of the ossification front and increases bone mineral deposition at the site of load application.

Lower femoral head coverage was associated with a greater z-axis height (increased bending) at 32 weeks. There was evidence that the SCO was also thinner in this region for lower femoral head coverage. The location of this bend in the m-rep medial mesh was lateral to the superior, perifoveal region that is the typical site of focal,

Table 3.6 Test statistics for normalized z-axis height at 32 weeks and degeneration score.

atom	χ^2 (1 df)	*p*-value
0,3	6.45	0.011
2,4	6.66	0.010
3,3	7.00	0.008
3,4	6.33	0.012
4,2	4.95	0.026
5,1	4.28	0.039
5,2	4.03	0.045

eccentric loading in subluxated hips. The bend in the m-rep mesh represents the more global effect on SCO shape due to subluxation.

A limitation of this study was the small sample size; however, the effects of lower femoral head coverage on SCO shape were strong enough to be detected at the 0.05 significance level. Spatial correspondence between atoms from m-reps at 14 and 32 weeks was assumed. A mesh regularity penalty and shape-relative landmarks were used during m-rep fitting to establish positional correspondence (26). The reduced radius was in the same, and expected, location for the 14- and 32-week m-reps, suggesting that the assumption of spatial correspondence was reasonable.

To our knowledge, this is the first study to perform a detailed *in vivo*, noninvasive evaluation of femoral head shape development in either an animal model or human DDH. The femoral head was thinner in the superior, perifoveal region and exhibited a

lateral bend. Our results demonstrate that chronic subluxation alters the adult morphology of the femoral head in what appears to be a dose-response pattern. Finite element models have shown that subtle abnormalities in hip morphology are associated with an increased risk for early OA onset (2–4). Further detailed shape analysis of the advancing ossification front will improve our understanding of how joint articulation during development affects adult hip morphology and will improve our ability to detect hips at risk of early onset OA.

Acknowledgments

The authors thank Dr. Stephen Pizer for providing the Binary Pablo software and Drs. Gregg Tracton and Graham Gash for technical support and much practical advice. The authors also thank Dr. Nathan Dykes for access to the CT scanner and the Baker Institute for Animal Health, Cornell University, for access to the Labrador retriever breeding colony. Support (W.S.V.B.-F.) was received from NSF and AAUW fellowships, and research was funded by a Cornell University College of Veterinary Medicine Consolidated Research Grant and New York State Advanced Technology Biotechnology Program Grant.

REFERENCES

1. Ogden JA 1982 Dynamic pathobiology of congenital hip dysplasia. In: Tachdjian MO (ed) Congenital Dislocation of the Hip. Churchill Livingstone, New York, pp 93-144

2. Russell ME, Shivanna KH, Grosland NM, Pedersen DR 2006 Cartilage contact pressure elevations in dysplastic hips: a chronic overload model. J Orthop Surg 1:6

3. Hadley NA, Brown TD, Weinstein SL 1990 The effects of contact pressure elevations and aseptic necrosis on the long-term outcome of congenital hip dislocation. J Orthop Res 8:504-513

4. Maxian TA, Brown TD, Weinstein SL 1995 Chronic stress tolerance levels for human articular cartilage – 2 nonuniform contact models applied to long-term follow-up of CDH. J Biomech 28: 159-166

5. Weinstein SL 1987 Natural history of congenital hip dislocation (CDH) and hip dysplasia. Clin Orthop Relat Res 225:62-76

6. Shipman SA, Helfand M, Moyer VA, Yawn BP 2006 Screening for developmental dysplasia of the hip: a systematic literature review for the US Preventative Services Task Force. Pediatrics 117:e557-e576

7. Committee on Quality Improvement, Subcommittee on Developmental Dysplasia of the Hip 2000 Clinical practice guideline: early detection of developmental dysplasia of the hip. Pediatrics 105:896-905

8. McLeod KJ, Rubin CT, Otter MW, Qin YX 1998 Skeletal cell stresses and bone adaptation. Am J Med Sci 316:176-183

9. Jee WSS 2001 Integrated bone tissue physiology: anatomy and physiology. In: Cowin SC (ed) Bone Mechanics Handbook. CRC Press LLC, Boca Raton, pp 1.1-1.68

10. Vanden Berg-Foels WS, Schwager SJ, Todhunter RJ, Reeves AP 2007 Femoral head bone mineral density patterns are altered by subluxation during development

in a canine model of DDH. Unpublished material, Cornell University, Ithaca, New York

11. Chalmers J, Ray RD 1962 The growth of transplanted foetal bones in different immunological environments. J Bone Joint Surg Br 44: 149-164

12. Harrison TJ 1961 The influence of the femoral head on pelvic growth and acetabular form in the rat. J Anat 95:12-26

13. Langenskiöld A, Shapiro O, Michelsson JE 1962 Experimental dislocation of the hip in the rabbit. J Bone Joint Surg Br 44:209-215

14. Schoenecker PL, Lesker PA, Ogata K 1984 A dynamic canine model of experimental hip dysplasia. Gross and histological pathology, and the effect of position of immobilization on capital femoral epiphyseal blood flow. J Bone Joint Surg Am 66:1281-1288

15. Smith WS, Ireton RJ, Coleman CR 1958 Sequelae of experimental dislocation of a weight-bearing ball-and-socket joint in a young growing animal: gross alterations in bone and cartilage. J Bone Joint Surg Am 40: 1121-1127

16. Riser WH 1975 The dog as a model for the study of hip dysplasia. Growth, form, and development of the normal and dysplastic hip joint. Vet Pathol 12:234-334

17. Lust G 1993 Other orthopedic diseases: hip dysplasia in dogs. In: Slater D (ed) Textbook of Small Animal Surgery. WB Saunders Company, Philadelphia, pp 1938-1944

18. Vanden Berg-Foels WS, Todhunter RJ, Schwager SJ, Reeves AP 2006 Effect of early postnatal body weight on femoral head ossification onset and hip osteoarthritis in a canine model of developmental dysplasia of the hip. Pediatr Res 60:549-554

19. Farese JP, Todhunter RJ, Lust G, Williams AJ, Dykes NL 1998 Dorsolateral subluxation of hip joints in dogs measured in a weight-bearing position with radiography and computed tomography. Vet Surg 27:393-405

20. Todhunter RJ, Bertram JE, Smith S, Farese JP, Williams AJ, Manocchia A, Erb HN, Dykes NL, Burton-Wurster NI, Lust G 2003 Effect of dorsal hip loading, sedation, and general anesthesia on the dorsolateral subluxation score in dogs. Vet Surg 32:196-205

21. Lust G, Todhunter RJ, Erb HN, Dykes NL, Williams AJ, Burton-Wurster NI, Farese JP 2001 Repeatability of dorsolateral subluxation scores in dogs and correlation with macroscopic appearance of hip osteoarthritis. Am J Vet Res 62:1711-1715

22. Reeves AP, Prokop RJ, Andrews SE, Kuhl FP 1988 Three-dimensional shape analysis using moments and Fourier descriptors. IEEE Trans Pattern Anal Mach Intell 10:937-943

23. Kostis WJ, Reeves AP, Yankelevitz DF, Henschke CI 2003 Three-dimensional segmentation and growth-rate estimation of small pulmonary nodules in helical CT images. IEEE Trans Med Imaging 22:1259-1274

24. Pizer S, Siddiqi K, Yushkevich PA 2007 Introduction. In: Siddiqi K, Pizer SM (eds) Medial representations: mathematics, algorithms and applications. Klewer Academic Publishers, Boston, pp 1-52

25. Pizer SM, Fritsch DS, Yushkevich P, Johnson V, Chaney E 1999 Segmentation, registration and measurement of shape variability via image object shape. IEEE Trans Med Imaging 18:851-865

26. Pizer S, Han Q, Joshi S, Fletcher PT, Yushkevich PA, Thall A 2007 Synthesis, deformation, and statistics of 3D objects via m-reps. In: Siddiqi K, Pizer SM (eds) Medial representations: mathematics, algorithms and applications. Klewer Academic Publishers, Boston, pp 311-342

27. Merck D, Tracton G, Pizer S, Joshi S 2006 A methodology for constructing geometric priors and likelihoods for deformable shape models. Manuscript submitted for publication

28. Fletcher P, Lu C, Pizer S, Joshi S 2004 Principal geodesic analysis for the study of nonlinear statistics of shape. IEEE Trans Med Imaging 23:995-1005

29. Pizer S, Styner M, Terriberry T, Broadhurst P, Joshi S, Chaney E, Fletcher PT 2007 Statistical applications with deformable m-reps: anatomic object segmentation and discrimination. In: Siddiqi K, Pizer SM (eds) Medial representations: mathematics, algorithms and applications. Klewer Academic Publishers, Boston, pp 343-396

30. Raudenbush SW, Bryk AS 2002 Hierarchical linear models: applications and data analysis methods. Sage, Thousand Oaks, pp 228-251

31. Searle SR, Casella G, McCulloch CE 1992 Variance components. John Wiley & Sons, Inc, New York, pp 1-18

32. Agresti A 2002 Categorical data analysis. JohnWiley & Sons, Inc, Hoboken, pp 274-282

33. Littell RC 2003 Analysis of unbalanced mixed model data: a case study comparison of ANOVA versus REML/GLS. J Agric Biol Environ Stat 7:472-490

34. Burton-Wurster N, Farese JP, Todhunter RJ, Lust G 1999 Site-specific variation in femoral head cartilage composition in dogs at high and low risk for development of osteoarthritis: insights into cartilage degeneration. Osteoarthritis Cartilage 7:486-497